Abstract

A thorough understanding of the influence of the addition of natural fibers on the water absorption and solubility of bio-based composites is of importance in tailoring its performance in a wet environment. In this study, PLA/sisal biocomposites were prepared by compression moulding for different amounts of fiber. An accelerated hydrothermal degrading test was designed for several temperatures above the glass transition to analyse the behaviour of water absorption of PLA/sisal biocomposites. The diffusion coefficients and percentage of water at saturation for different hydrothermal conditions were characterized in terms of fiber content (10, 20 and 30%) and the use of maleic anhydride as a coupling agent. Microstructural changes occurred during and after the water absorption process were evaluated by thermal analysis and electron microscopy. Non-significant chemical changes were found in terms of back-bone chain scission. Surface analysis showed an important physical degradation promoted by the formation of microcracks around swollen fibers. This effect was more relevant the higher the fiber content was. As well, the use of maleic anhydride used as a coupling agent slightly promoted smaller cracks on PLA/sisal biocomposites.

Contents

Glossary

Abbreviations

CA	Coupling Agent
DCP	Dicumyl Peroxide
DSC	Differential Scanning Calorimetry
DTG	Derivative Thermo-Gravimetrý
MA	Maleic Acid
PLA	Poly(lactide)
PLA10	Poly(lactide) + 10% sisal fiber
PLA10C	Poly(lactide) + 10% sisal fiber + Coupling Agent
PLA20	Poly(lactide) + 20% sisal fiber
PLA20C	Poly(lactide) + 20% sisal fiber + Coupling Agent
PLA30	Poly(lactide) + 30% sisal fiber
PLA30C	Poly(lactide) + 30% sisal fiber + Coupling Agent
SEM	Scanning Electron Microscopy
TG	Thermo-Gravimetry
TGA	Thermo Gravimetric Analysis
VPLA	Virgin Poly(lactide)

Symbology

C	Concentration of penetrating agent
D	Diffusion coefficient
J	Penetrating flux per unit area
l	Thickness of the specimen
m_0	Specimen mass after initial drying
m_1	Specimen mass after immersion
m_P	Polymer matrix weight in composite
m_∞	Specimen mass at equilibrium
M_t	Water uptake at time t
M_s	Water saturation mass
P	Permeation coefficient
S	Sorption coefficient
t	Time
T_c	Crystallisation temperature peak
T_{cc1}	First cold crystallisation temperature peak
T_{cc2}	Second cold crystallisation temperature peak
T_g	Glass transition temperature
$T_{g\text{-}p}$	Peak temperature associated to glass transition relaxation
T_{HA}	Hydrothermal condition
T_m	Melting temperature peal
T_{md}	Main degradation peak
T_o	Onset temperature
q	Specific heat

Xc	Crystallinity degree
Xc_s	Saturation crystallinity degree
Θ	Slope of M_t/M_s vs $t^{1/2}$
Δcp	Specific heat associated to glass transition
ΔH_c	Enthalpy associated to crystallisation
ΔH_{cc1}	Enthalpy associated to first cold crystallisation
ΔH_{cc2}	Enthalpy associated to second cold crystallisation
ΔH_{gt}	Enthalpy associated to glass transition relaxation
ΔH_m	Enthalpy associated to melting
ΔH_0	Enthalpy of fusion for a 100% crystalline sample

1. Introduction

1.1 Motivation and aim

Plastics account for about 20% by volume of municipal solid waste (MSW). Many cities have exhausted the available space for this waste material and considered management models that dissociate the production site from the garbage disposal site. Therefore, one is paying for shipping waste to remote areas of the municipalities of origin. Furthermore, not only is creating so much waste that no one knows what to do with, but also are becoming extinct finite natural resources. It is estimated that the global resources of oil, natural gas and coal are limited and the economic impact could be felt exhausted in the next 50 years, as prices will rise as these resources are exhausted [1].

Due to rising oil prices and the problem of the accumulation of waste, which has led to very stringent environmental policies, scientists are developing biodegradable plastics made from renewable resources, such as poly (lactic acid) or polylactide (from now on, PLA) [2,3].

PLA is a highly versatile, biodegradable polymer produced from agricultural bases such as corn, beets, wheat and other starchy products. Lactic acid is a chiral molecule, and presents optical isomerism, having four morphologically different isomers: two stereo regular shapes, D-lactic and L-lactic acid, and racemic D,L and L,D-lactic acid. Figure 1 shows the differences between the isomeric forms that may be present lactic acid. PLA is commonly synthetized by two methods: by ring-opening polymerization of lactide and by direct polycondensation of lactic acid [4].

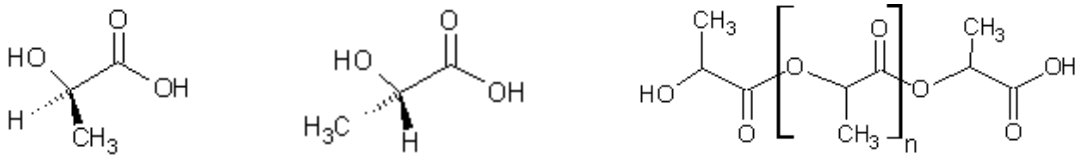

Figure 1. D and L-lactic acid and PLA.

PLA has been used as package material and medical products, due to its high strength, thermal properties and biocompatibility [5]. In order to improve the mechanical and thermal properties of PLA, some fibers or fillers can be added, which provide reinforcement properties at lower cost, lower density and higher strength and stiffness [6,7]. The potential advantages of natural fibers have been well documented and are generally based on environmental friendliness as well as health and safety factors [8,9].

Sisal fiber is a commonly filler used in composites. Sisal plant (*Agave sisalana*) is an agave that yields a stiff fibre traditionally used in making twine and rope. It looks like a giant pineapple, as can be seen in Figure 2.

Figure 2. Sisal plant (*Agave sisalana*) and woven sisal fiber.

Nevertheless, natural fibers, due to their chemical constituents, usually attract water and humidity because of their hygroscopic nature. It has been studied that the moisture absorption by composites containing natural fibers has numerous adverse effects on their structure and properties and thus affects their long-term behaviour. For example, an increase in humidity decreases their mechanical properties, and changes their dimensions [10-12]. Numerous efforts have been made to address this issue. Coupling agents, compatibilizers or other chemical modifications are usually used to improve the moisture resistance of composites with natural fibers [13-15].

The consequences of the water absorption phenomenon can be predicted by an accelerated hydrodegradation process, for example [16]. An essential understanding of the PLA degradation process and morphological behaviour during the degradation is crucial for material development and extending the application of this sustainable polymer, especially in packaging.

The aim of this study was to understand the influence of the temperature, amount of sisal fiber and presence of coupling agent on water absorption of reinforced PLA biocomposites. A model of an accelerated hydrothermal degradation was designed for several temperatures above glass transition, obtaining the water absorption processes in terms of diffusion coefficients and percentage saturation. Monitoring the water absorption course was thought as a way to understand how the structure of the biocomposites changes along the whole process. Thermal analysis and electron microscopy were considered as good methods to study physico-chemical properties.

1.2 Theoretical approach

1.2.1 Water uptake in biocomposites

Polymer composites, especially those reinforced with natural fiber, are able to absorb moisture when they are immersed in water [17], which may affect the fiber/matrix interface leading to hydrodegradation. Moreover, moisture absorption by natural fibers affects their physical and chemical properties [18].

The component responsible for moisture absorption in natural fibers is associated with cellulose [19]. It consists in relative low molecular weight polysaccharides made from hexoses, pentoses, and uronic acid residues. Higher content of cellulose causes higher moisture sorption and subsequently higher biodegradation.

Diffusion coefficient (*D*), related to the ability of solvent molecules to move among the polymer segments, is used to characterise the water absorption process. When the temperature of the moisture environment rises, it develops microcracks on the surface and in the bulk of the material. This results in the increase of the permeability phenomenon [20].

There are three different mechanisms that can facilitate the transport of water: diffusion inside the matrix, by imperfections within the matrix (microspaces, pores or cracks); or by capillarity along the fibre/matrix interface [21,22].

Water absorbed in composites consists in free water and bound water [23]. As Figure 1.1 shows, free absorbed water are molecules able to self-move through voids while bound water are dispersed molecules bounded to the polar groups of both polymers and fibers.

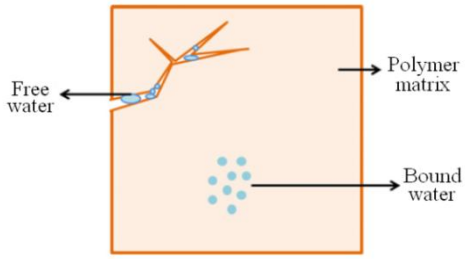

Figure 1.1. Free and bound water – Adapted from [24].

Water adhesion in hydrophilic groups of fibers establishes intermolecular hydrogen bonding with them and reduces interfacial adhesion of fiber/matrix. Degradation phenomenon occurs when cellulose fibers develop stress at interface regions after water absorption, leading to

microcracking mechanism in the matrix around swollen fibers, which in turn promotes capillarity and transport via microcracks. Water soluble constituents start leaching from fibers and finally lead to a debonding effect between fiber and matrix. It is initiated by the development of osmotic pressure pockets at the surface of fibers due to the leaching of water soluble substances [20]. This process is summarised in Figure 1.2.

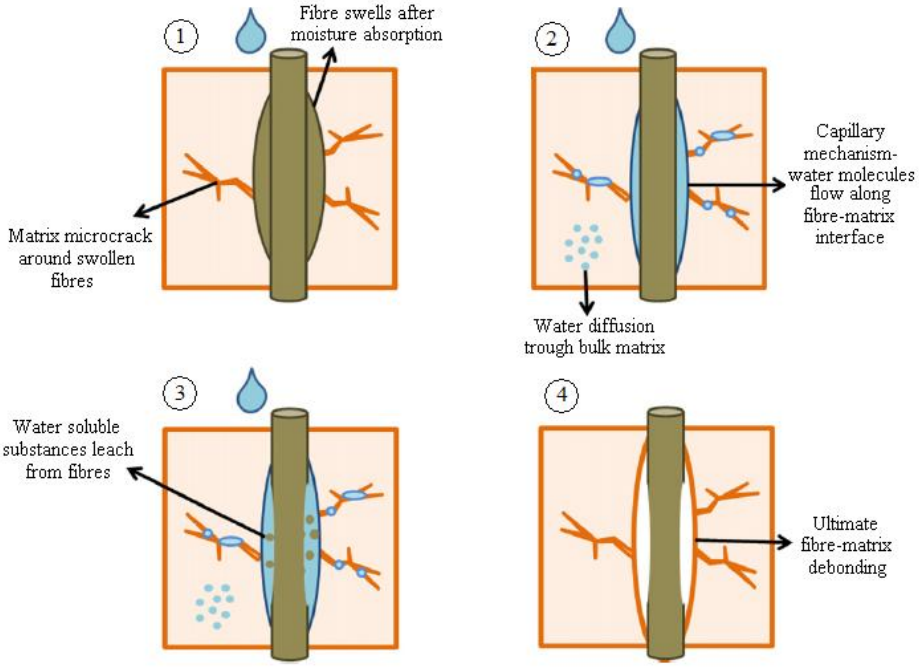

Figure 1.2. Debonding phenomenon between fiber and matrix – Adapted from [24].

The characteristics of natural fibre composites immersed in water are influenced by the nature of the fibre and matrix materials, by the relative humidity and manufacturing technique [18].

The manner in which composite materials absorb water depends upon several factors such as temperature, fibre volume fraction, orientation of reinforcement, permeability, nature of fibre, area of exposed surfaces, diffusivity, reaction between water and matrix and surface protection [20].

1.2.2 Fluid transport process in composites

When molecules of condensable vapour, a gas or a liquid, as water in this case, permeate through a membrane or polymer sheet, the overall process is the result of two distinct processes: the sorption of the fluid in the exposed face polymeric material and subsequent diffusion of such small molecules across the sheet. The joint consideration of both phenomena which results in permeability means, involves the overall traffic penetrating from one side of the polymeric material to the other in a given time period and at a specific pressure [25].

Traditionally, the diffusion theory has been applied to understand the mechanism of moisture absorption in composites. Diffusion process is kinetic concepts that can be considered as a statistical molecular transport, due to the random movement of molecules possess [25-27].

The simplest way to describe phenomenological diffusion is Fick's first law (Equation 1.1).

$$J = -D\frac{\partial C}{\partial x} \qquad (1.1)$$

where J is the penetrating flux per unit area, C is the concentration of penetrating and x the walking space penetrant. Considering the mass balance in a volume element, Equation 1.1 takes the form of Equation 1.2,

$$\frac{\partial C}{\partial t} = D\left(\frac{\partial^2 C}{\partial x^2} + \frac{\partial^2 C}{\partial y^2} + \frac{\partial^2 C}{\partial z^2}\right) \qquad (1.2)$$

where t is time and x, y and z are the space that runs through the piercing in each direction of space.

In this case, the diffusion coefficient D is independent on the penetrant concentration and constant. However, in many cases D depends upon the diffusion of penetrant concentration. This fact, which usually occurs when the medium is not homogeneous, D varies from one point to the next, so that Equation 1.2 takes the form of Equation 1.3,

$$\frac{\partial C}{\partial t} = \frac{\partial}{\partial x}\left(D\frac{\partial C}{\partial x}\right) + \frac{\partial}{\partial y}\left(D\frac{\partial C}{\partial y}\right) + \frac{\partial}{\partial z}\left(D\frac{\partial C}{\partial z}\right) \qquad (1.3)$$

where D may be a function of the coordinates and of the concentration C.

Often diffusion occurs in only one direction, so that Equation 1.3, it becomes what is known as Fick's second law in Equation 1.4,

$$\frac{\partial C}{\partial t} = \frac{\partial}{\partial x}\left(D\frac{\partial C}{\partial x}\right) \tag{1.4}$$

which can be converted into Equation 1.5,

$$\frac{\partial C}{\partial t} = D\left(\frac{\partial^2 C}{\partial x^2}\right) \tag{1.5}$$

These solutions Fick's laws for diffusion are different depending on the experimental conditions that perform the calculation of the diffusion coefficient, or on the geometric structure of the material under study.

For plane sheet geometry, the liquid concentration in the composite at time *t* is given by Equation 1.6,

$$\frac{C_t}{C_\infty} = 1 - \frac{4}{\pi}\sum_{n=0}^{\infty}\frac{1}{2n+1} \times \exp\left[-D\frac{(2n+1)^2\pi^2}{l^2}t\right]\sin\left[\frac{(2n+1)\pi}{l}x\right] \tag{1.6}$$

where l is the thickness of the specimen, and C_∞ the concentration of the liquid in the composite at equilibrium.

If the mass uptake at time *t* is used as M_t and the water uptake at the equilibrium as M_s, it can be simplified using Stefan's approximation (Equation 1.7). This estimation is used for describing the earlier stages of water uptake, usually where $M_t/M_s \leq 0.5$.

$$\frac{M_t}{M_s} = \frac{4}{l}\left(\frac{Dt}{\pi}\right)^{1/2} \tag{1.7}$$

where D is the diffusion coefficient and l is the thickness of the sample. By representing the M_t/M_s ratios as a function of the square root of time, it can be calculated Θ, the slope of the plot. So the diffusion constant (D) can be calculated according to the Equation 1.8.

$$D = 0.0625\pi l^2\theta^2 \tag{1.8}$$

In order to understand the degree of interaction between water and polymer due to the introduction of sisal fiber making a composite, it can be calculated the sorption coefficient *S*. This parameter can be calculated on the polymer phase using Equation 1.9.

$$S = \frac{(m_s - m_0)}{m_p} \qquad (1.9)$$

where m_p is the polymer matrix weight in the composite, m_s is the weight of the specimen at the equilibrium.

The permeation coefficient *P* is the transport rate of diffusants to penetrate through the material's thickness under specified temperature and humidity conditions. It is a function of sorption and diffusion, and can be determined by combining the diffusion coefficient, *D* and sorption coefficient, *S* in Equation 1.10.

$$P = D \cdot S \qquad (1.10)$$

This equation shows that the permeability is a process that will directly depend on the affinity between penetrant and polymer, and on the penetrant progress along the thickness of the polymer sample. However, the permeability is not an intrinsic property for a given polymer. That is, the permeability coefficient for a given pair penetrant-polymer will be different if varying factors such as pressure at which the experiment is performed, morphology of the sample or experimental device used for measurement [25-27].

1.2.3 PLA/sisal biocomposites hydrolysis

The hydrolytic degradation of PLA matrix under hydrothermal conditions proceeds through random cleavage of the ester bond. Four basic parameters control this process: the rate constant, the amount of absorbed water, the diffusion coefficient of chain fragments within the polymer and the solubility of degradation products [28].

The degradation of a solid polymer matrix can proceed through two alternative mechanisms: surface or heterogeneous, and bulk or homogeneous erosion [29]. In the first case, the polymer degradation is much faster than water intrusion into the polymer bulk. Degradation occurs, therefore, mainly in the outermost polymer layers and not in the inner parts of a matrix. Bulk eroding polymers, in contrast, degrade slowly and water uptake by the system is much faster than polymer degradation. Thus the entire system is rapidly hydrated and the polymer chains are cleaved throughout the device. However, it should be noted that all degradable polymers can erode via both pathways when the erosion conditions or the geometry are chosen appropriately. Degradation becomes a bulk process above glass transition, while at temperatures below T_g degradation of the polymer matrix is restricted to its surface [34].

The hydrolytic degradation of semi-crystalline PLA matrices proceeds in two stages, as reported by Fischer et al. [31]. During the first stage, water diffuses into the amorphous phase resulting in random hydrolytic scission of ester bonds. The degree of crystallinity can even increase as degradation proceeds. The second stage starts after degradation of the major part of the amorphous area. The hydrolytic attack proceeds from the edge towards the centre of crystalline domains.

Additional parameters that influence hydrolysis are the temperature and pH of the solution [32-34]. The mode of scission during hydrolysis of biodegradable polymers could be completely random regarding the backbone bonds or it could follow a “chain-end-unzipping” mechanism. It was found that the base catalysed hydrolysis of D,L-PLA proceeds via a random process, while the acid catalysed hydrolysis follows a fast chain-end scission [33]. It was also established that the hydrolysis rate is higher in acidic than in neutral media [32].

The hydrolysis reaction of PLA can be expressed as follows [35]:

$$-CHCH_3COO- + H_2O \rightarrow -CHCH_3OH + HOOC-$$

$-CHCH_3COO-$ groups on PLA molecule react with H_2O and form low molecular weight products; thereby breakage of PLA molecular chain occurs.

On the moisture effect, the mechanical properties of natural fibre reinforced composites can be reduced to a great extent under moist conditions [36-40]. Natural fibers seem to have little resistance towards environmental influences. This can be recognised in the composite and can be advantageously utilised for the development of biological degradable composites with good physical properties [41]. Cellulose fibers are difficult to dissolve because of their high crystallinity, however, they tend to retain liquids in the interfibrillar space. This is a serious concern as there are potential outdoor or packaging applications, where moisture absorptions can have significant influence for these materials. The interfacial bonds between the natural fibers (which contain hydroxyl and other polar groups) and the relatively hydrophobic polymer matrices would be weakened with high water uptake. The weakened interface causes the reduction of the mechanical properties of the composites.

2. Materials and methods

2.1 Materials and preparation of PLA/sisal biocomposites

PLA pellets (Grade 3251D) from Nature Works (Minnetonka, USA) and sisal fibre (length 0.5 – 1 mm) were dried in an oven at 80 ^{o}C at least 12 hours and kept in zip bags to prevent the presence of moisture during processing. The fibre contents in the biocomposite were formulated as 10%, 20% and 30% by weight. In case of using coupling agent (CA), maleic anhydride (MA) 2.5% and dicumyl peroxide (DCP) 0.3% were added. All materials were mixed in an internal mixer (Brabender, Germany) during 5 minutes at 180 ^{o}C and 50 rpm of speed.

The compounded fibre/PLA biocomposite was ground by means of a grinder. These granules were dried at 80 ^{o}C in the oven at least 12 hours before further compression moulding, in order to avoid the hydrolysis degradation by moisture during the thermal process. Squared 100 mm^2 biocomposite sheets were fabricated by using a compression moulding (Fontijne Presses, Netherlands). The sheet shaped biocomposites preparation procedure consisted on preheating the press to 200 ºC for 2 min, applying of compression force 150 kN and maintaining it for 2 min. All the operations were performed under vacuum condition. All compounded biocomposites were dried by vacuum oven at 80 ºC at least 4 hours and then put in zip bags and placed in a desiccator. The thickness of the sheet samples was 0.5± 0.1 mm.

This biocomposites sheets were cut into small and manageable sizes as shown in Figure 2.1.

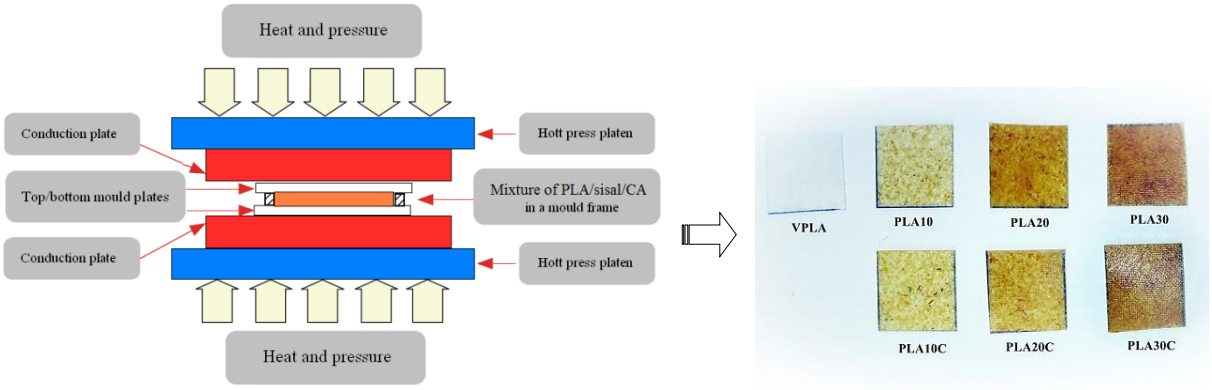

Figure 2.1. Compression moulding scheme –adapted from [24]– and PLA/sisal biocomposites sheets.

2.2 Water absorption

To carry out hydrothermal assay, a standard test of water absorption was taken as a reference. From a physicochemical perspective, the strictest procedure involves gravimetric monitoring of the amount of penetrant retained by the composite. The standard based in the UNE-EN-ISO 62:2008 Plastics. Determination of water absorption [42] describes a method for determining moisture absorption properties in the direction "across the thickness" of flat solid plastics. The coefficient of diffusion of moisture through the thickness can be determined in a single phase material assuming diffusion behaviour according to Fick's law.

According to the standard, tests have to be performed by immersing specimens into distilled water at 23 °C or boiling in distilled water, or exposing them to 50% relative humidity, at defined temperatures for specified periods of time. This study used a modification of the experimental procedure, so the sample was immersed at several temperatures above the glass transition of the polymer: 60, 65, 70, 75, 80 and 85 ºC. The size of these samples, generally, was 20 ± 1 mm in length, 20 ± 1 mm wide and thickness 1 ± 0 mm. The test time for each temperature corresponded to three times the saturation time of the material with slower saturation rate, so the duration of the test is estimated as $3 \cdot t_{saturation}$.

All samples were dried in an oven at 50 ± 2 °C (Heraeus Vacutherm 6025) for at least 24 h and cooled to room temperature in a desiccator before weighing specimens approaching 0.1 mg (mass m_1) (Mettler Toledo AB135-S). During weighing, the samples did not absorb nor desorb any water. It was immediately measured after being taken from exposure environment.

Then the specimens were placed in a container filled with distilled water maintained at the desired temperature (Heraeus Unitronic 200). After immersion for a certain time, the specimens were taken from the water and removed all traces of water surface with a clean dry cloth. Samples were weighed again approaching 0.1 mg within 1 min after water removal (mass m_2). The water content at the saturation point was determined by immersing the specimen again, and repeating weighing process until reaching $3 \cdot t_{saturation}$.

To calculate the percentage of water absorbed mass (M_t) for each sample is used Equation 2.1:

$$M_t(\%) = \frac{m_1 - m_0}{m_0} \times 100 \qquad (2.1)$$

where m_0 is the mass of the specimen before immersion, and m_1 is the mass after immersion.

2.3 Thermal behaviour

With the aim of reducing the number of thermal analysis assays without reducing the scope of the results, it was decided to analyse only the hydrothermal conditions of 65, 75 and 85 ° C.

2.3.1 Thermo-Gravimetric Analysis (TGA)

Thermal stability data were obtained by Thermo-Gravimetry by means of a Mettler-Toledo TGA 851 series. The samples, with a mass of about 4 mg were introduced in TGA Mettler-Toledo perforated alumina crucibles, with capacity of 70 µl. Three specimens of each sample were analysed by a dynamic thermo-gravimetric procedure, with a heating rate of 10 ° C/min in the temperature range of 25 to 800 °C, under oxidative atmosphere of oxygen at a flow rate of 50 ml/min.

2.3.2 Differential Scanning Calorimetry (DSC)

Calorimetric data were obtained by Differential Scanning Calorimetry by means of a Mettler-Toledo DSC 820 series equipped with a refrigerated cooling system (RCS). Prior to the tests, the DSC equipment was calibrated following the procedure of In and Zn. Calorimetric analysis was performed with a heating/cooling rate of 10 °C/min. The samples, with a mass of about 4 mg were placed in an aluminium crucible perforated on top, with capacity of 40 µl. Structural changes were assessed over the first heating ramp, held at 10 °C/min, between 0 and 200 °C. Degradation effects were evaluated over the second heating ramp, held at 10 ºC/min between 0 and 200 ºC too. All experiments were performed using N_2 as protective gas (50 ml/min).

DSC analyses were performed with the aid of the software STARe 9.10 from Mettler-Toledo. The specimens were characterized at least by triplicate and the averages of temperatures and enthalpies were taken as representative values.

2.4 Morphological study

2.4.1 Scanning Electron Microscopy (SEM)

The surface morphology of the specimens was analysed by means of a Hitachi S-4800 Field Emission Scanning Electron Microscope (Tokyo, Japan). The samples were cut into small pieces and dried at 50 ºC for 24 h and then kept in desiccator for 48 h before SEM sample preparation. The pieces were mounted on metal studs and sputter-coated with a 2 nm gold layer using a Cressington 208HR, high resolution sputter coater (Watford, UK), equipped with a Cressington thickness monitor controller.

3. Results and discussion

3.1 Water uptake

The absorption curves resulting from hydrodegradation process along exposure time at different temperatures are shown in Figure 3.1. Note that the values represented exhibit a deviation between 3 and 5%.

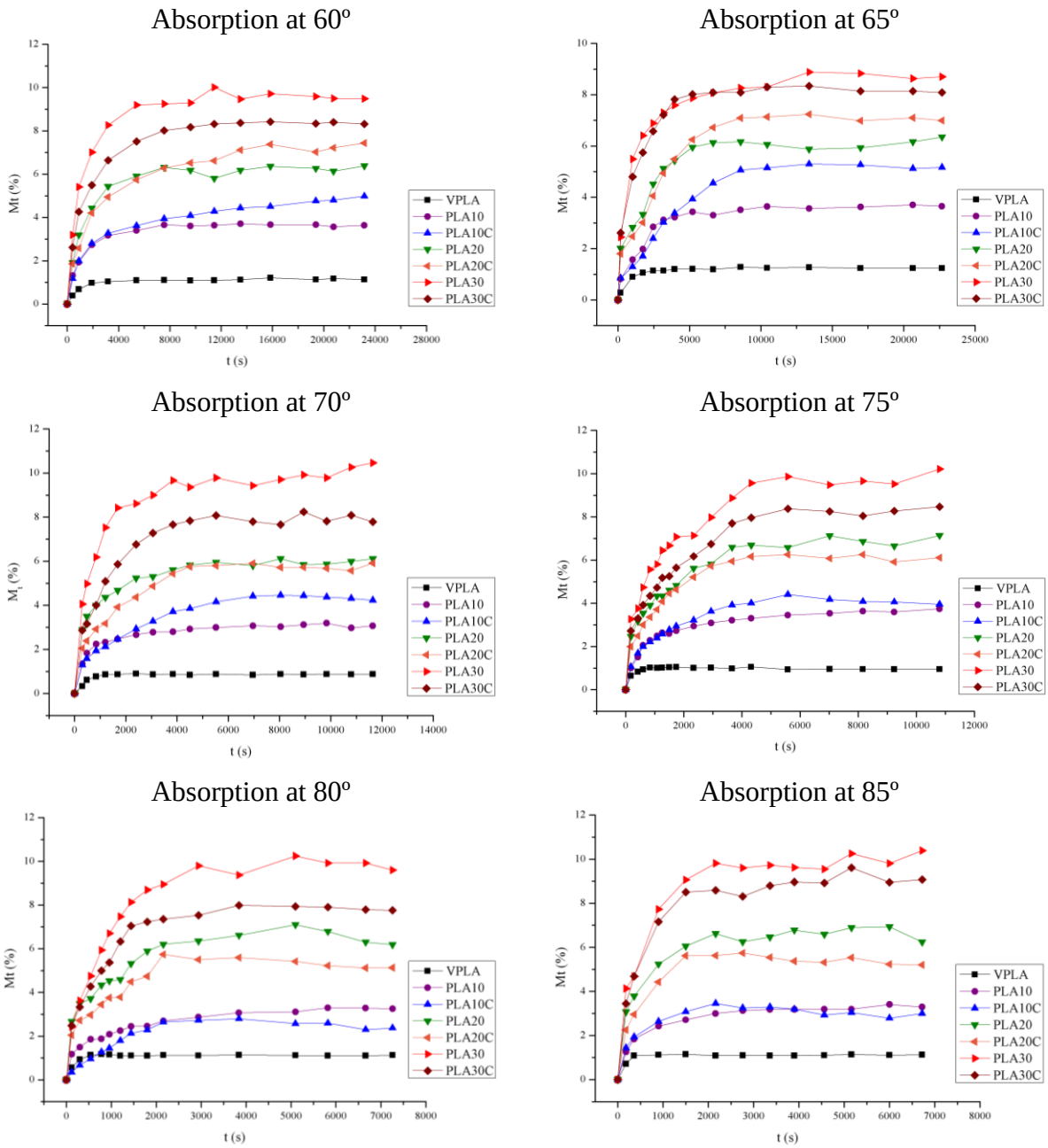

Figure 3.1. Plots of M_t against t for PLA and composites for all hydrothermal conditions.

Water absorption increased as the immersion time did until equilibrium was achieved. All of these sorption curves display two phases: fast sorption at the initial stage and slow sorption thereafter, followed by asymptotic saturation. A global tendency was observed for all cases. This is in accordance with most of the moisture absorption studies on natural fiber composites [43, 46 and 48].

The values of the water mass absorbed M_s for different compositions and temperatures are gathered at Table 3.1.

Table 3.1. Water saturation mass (M_s) for all hydrothermal conditions.

M_s (%)	**Hydrothermal condition (ºC)**											
	60		**65**		**70**		**75**		**80**		**85**	
Fiber content (%f)	**Coupling agent**											
	Yes	**No**	**Yes**	**No**	**Yes**	**No**	**Yes**	**No**	**Yes**	**No**	**Yes**	**No**
0	1,1 (±0,1)		1,2 (±0,1)		0,8 (±0,02)		0,9 (±0,03)		1,1 (±0,1)		1,1 (±0,1)	
10	4,9 (±0,2)	3,6 (±0,1)	5,1 (±0,1)	3,6 (±0,1)	4,2 (±0,1)	3,0 (±0,1)	3,9 (±0,1)	3,7 (±0,1)	2,3 (±0,1)	3,2 (±0,1)	3,0 (±0,1)	3,2 (±0,1)
20	7,4 (±0,2)	6,3 (±0,2)	6,9 (±0,2)	6,3 (±0,2)	5,9 (±0,1)	6,1 (±0,3)	6,1 (±0,2)	7,1 (±0,3)	5,1 (±0,1)	6,1 (±0,1)	5,2 (±0,1)	6,2 (±0,2)
30	8,3 (±0,2)	9,4 (±0,2)	8,0 (±0,1)	8,7 (±0,2)	7,6 (±0,3)	10,4 (±0,4)	8,1 (±0,3)	9,3 (±0,4)	7,7 (±0,2)	9,6 (±0,3)	9,0 (±0,3)	10,3 (±0,2)

It is important to remark that the analysis of the results will be approached from three perspectives: amount of fiber (%f), presence of coupling agent (CA) and hydrothermal condition (temperature).

It can be seen from Table 3.1, for all temperatures, that VPLA has attained ~1%; the minimum value of water absorbed. Moreover, material with the major amount of absorbed water is always composite PLA30/30C, reaching ~10% of water. Values for VPLA are in consonance with other studies, as reported by Wang H. et al [44].

Sisal fiber in composites contributes to reach higher water saturation mass. Greater values in composites can be attributed to the hydrophilic nature of sisal fiber by virtue of the presence of an abundance of hydroxyl groups which are available for interaction with the water molecules [45]. As a result of fiber swelling, micro cracking of the polymer matrix could occur, as suggested by other authors [38]. As the composite cracks, could get damaged,

capillarity and transport via micro cracks can become active promoting more water penetration.

At a given temperature and amount of fiber, coupling agent influences differently for each case, so it can't established a general tendency. However, the material with the higher amount of water absorbed is always PLA30 without coupling agent.

There are not big changes in the amount of water absorbed for a given material at different temperatures: absorbed water amount is similar in all cases.

In order to simplify, clarify and confirm discussion and comments about the results, a statistic analysis was carried out. The results are observable in Figure 3.2 which shows the means of the M_s for all possible situations for the three different variables.

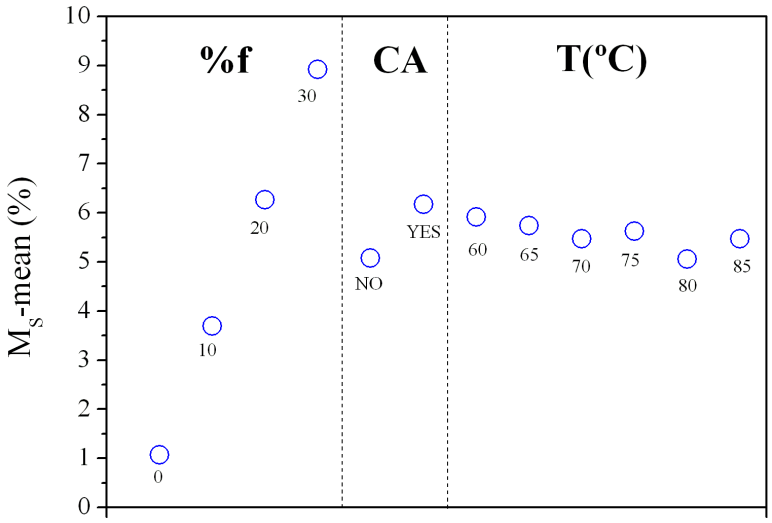

Figure 3.2. Plot of M_s-means versus fiber content, coupling agent and temperature.

The higher the amount of fiber, the more was the water absorbed mass. Moreover, it can be seen that the presence of the coupling agent slightly increased the amount of water absorbed. However, as it can be seen on the graph and we previously mentioned, temperature did not influence on the quantity of water absorbed.

To summarize the influence of the experiment variables on each other, there is an interaction plot in Figure 3.5, which gives a clearly vision and relations of the amount of water absorbed (M_s) and temperature, amount of fiber and presence of coupling agent.

3.2 Water transport parameters

In order to compare the differences on diffusion rates of the water absorption phenomenon reduced plots of water uptake for virgin PLA and composites for different temperatures are shown in Figure 3.3. Note that the values represented exhibit a deviation between 3 and 5%.

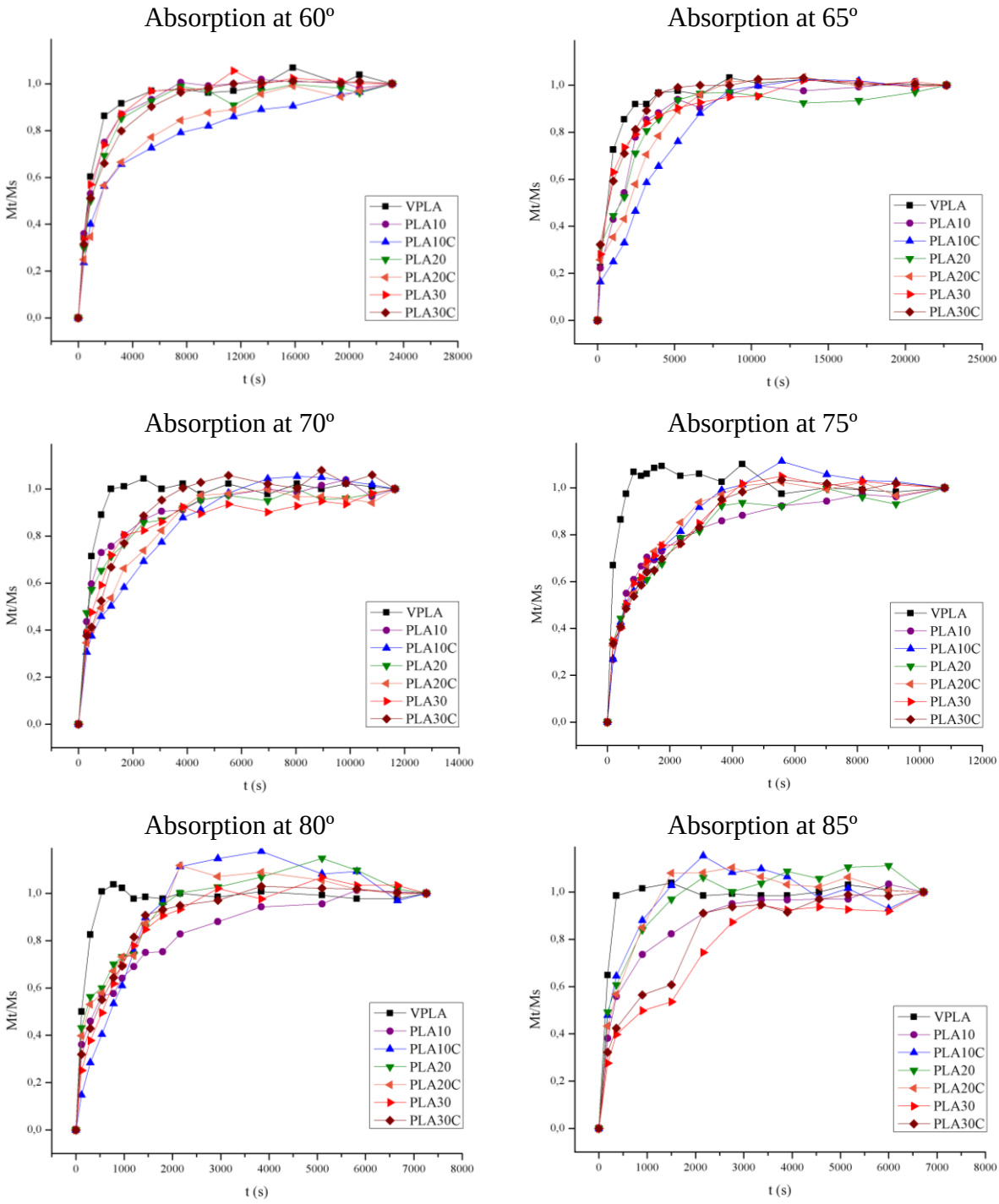

Figure 3.3. Plots of M_t/M_s against t for PLA and composites for all hydrothermal conditions.

Due to the effect of fiber on the composites water absorption, the saturation percentage M_s was reached by VPLA at earlier times than those given by composites.

Higher temperatures seem to accelerate the water uptake behaviour. When the temperature of immersion was increased, the water saturation time was greatly shortened (from ~8000 s at lower temperatures to ~3000 s at higher ones). The wide may be attributed to the different diffusion coefficient of water into the material. The diffusion coefficient D has been therefore assessed by means of Stefan's approximation (Equation 1.8) and the slope of the plot M_t/M_s versus square root of time for earlier stages of water uptake. Diffusion coefficients for several temperatures and materials are shown in Table 3.2. The obtained values are comparable to those reported for polylactide in previous studies [46].

Table 3.2. Diffusion coefficient D for all hydrothermal condition and amount of fiber.

D ·10^7 (cm^{2}s^{-1})	**Hydrothermal condition (ºC)**											
	60		**65**		**70**		**75**		**80**		**85**	
Fiber content (%f)	**Coupling agent**											
	Yes	**No**	**Yes**	**No**	**Yes**	**No**	**Yes**	**No**	**Yes**	**No**	**Yes**	**No**
0	1,7 (±0,1)		1,9 (±0,1)		3,7 (±0,1)		9,2 (±0,3)		9,1 (±0,4)		9,0 (±0,2)	
10	0,9 (±0,1)	1,6 (±0,1)	0,7 (±0,1)	2,3 (±0,1)	1,2 (±0,1)	3,1 (±0,1)	2,0 (±0,1)	2,2 (±0,1)	1,5 (±0,1)	3,3 (±0,1)	4,6 (±0,1)	4,5 (±0,2)
20	0,7 (±0,1)	1,4 (±0,1)	1,1 (±0,1)	1,6 (±0,1)	1,4 (±0,1)	2,5 (±0,1)	1,7 (±0,0)	1,7 (±0,1)	2,7 (±0,1)	2,7 (±0,1)	3,0 (±0,1)	3,1 (±0,1)
30	1,5 (±0,1)	1,6 (±0,1)	1,6 (±0,1)	1,7 (±0,1)	1,2 (±0,1)	2,1 (±0,1)	1,8 (±0,1)	2,1 (±0,1)	2,3 (±0,1)	2,1 (±0,1)	2,4 (±0,1)	2,1 (±0,1)

It can be seen from Table 3.2 that diffusion coefficient is temperature sensitive, being higher when it increases. These increment is larger for VPLA (from ~2 to ~9 ·10^{-7} cm^{2}s^{-1}) and decreases as rises the fiber content (for PLA30, from ~1.6 to ~2.2 ·10^{-7} cm^{2}s^{-1}). Even so, the addition of sisal fiber does not change the magnitude order of diffusion coefficient under the same temperature condition according to literature [49].

In order to clarify and quantify how the global tendencies for the means of *D* versus the three different variables were, a statistic study was performed as shown in Figure 3.4.

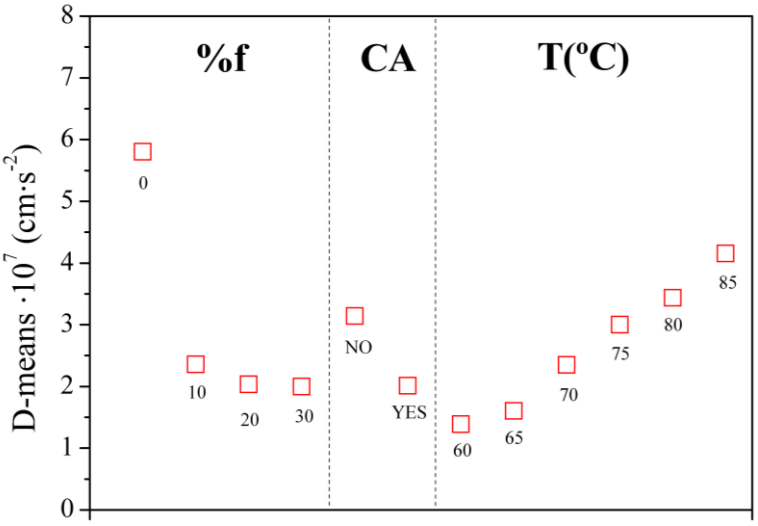

Figure 3.4. Plot of *D*-means versus fiber content, coupling agent and temperature.

In the case of inorganic fillers, *D* is reduced for composites due to the presence of sisal fiber. It could be based on the obstruction to the advance of penetrant along the composite sheet [48]. Although the hydrophilicity of fibers should indicate an increase of the diffusion coefficient, a reduction of *D* was shown. It suggested that some change is occurring in the internal structure of the composite. Previous studies for PLA demonstrated that the crystal growing could be the cause of diffusion coefficient reduction [46]. The transport paths of the water molecules and the water-interaction within the composite could be decreased, resulting in global lower diffusion coefficients.

Higher *D* for elevated temperatures is based on the fact that at high temperatures, openings among chains that are capable of accommodating the penetrant undergo rapid redistribution in space. A penetrant molecule resides in a certain position of the polymer matrix until the motion of surrounding chains, modified by the penetrant's presence, leads to the formation of a cavity, at a distance commensurate with the penetrant's diameter, into which the penetrant can move. After the move, the cavity in which penetrant was originally accommodated is closed. A succession of such small random moves of the penetrant constitutes diffusion. The higher is the temperature of the assay, the faster is the movement of polymer chains and higher is the diffusion coefficient [47].

The sorption coefficient *S* is helpful in understanding the interaction between water and the surface of the composite due to the introduction of sisal fiber. Thus, the capability of the composites to attract molecules of water to their surfaces can be assessed.

It was calculated for all materials too and hydrothermal conditions according to the Equation 1.9 and results are shown in Table 3.3.

Table 3.3. Sorption coefficient *S* for all hydrothermal condition and amount of fiber.

S (%)	**Hydrothermal condition (ºC)**											
	60		**65**		**70**		**75**		**80**		**85**	
Fiber content (%f)	**Coupling agent**											
	Yes	**No**	**Yes**	**No**	**Yes**	**No**	**Yes**	**No**	**Yes**	**No**	**Yes**	**No**
0	1,1 (±0,1)		1,2 (±0,1)		0,8 (±0,1)		0,9 (±0,1)		1,1 (±0,1)		1,1 (±0,1)	
10	5,6 (±0,2)	4,0 (±0,1)	5,9 (±0,2)	4,0 (±0,2)	4,8 (±0,1)	3,4 (±0,1)	4,5 (±0,1)	4,1 (±0,1)	2,7 (±0,0)	3,6 (±0,1)	3,4 (±0,1)	3,6 (±0,1)
20	9,3 (±0,3)	8,2 (±0,3)	8,7 (±0,3)	8,1 (±0,3)	7,4 (±0,2)	7,8 (±0,4)	7,6 (±0,2)	9,2 (±0,4)	6,4 (±0,2)	7,9 (±0,2)	6,5 (±0,2)	8,0 (±0,3)
30	12,3 (±0,3)	13,5 (±0,4)	11,9 (±0,2)	12,4 (±0,3)	11,3 (±0,5)	14,9 (±0,5)	12,0 (±0,5)	13,4 (±0,6)	11,4 (±0,4)	13,7 (±0,5)	13,4 (±0,5)	14,8 (±0,4)

The value of sorption coefficients does not change significantly for the different temperatures. However, it can be appreciated an increment on *S* when increases the amount of fiber in composites. Sorption coefficient goes from ~1% for VPLA to ~13% for composites with 30% of fiber. This increment is based on the hydrophilic nature of sisal fiber, which attracts much more water molecules than virgin PLA.

The permeation process involves two well-differenced steps. First one is sorption of the liquid molecules, water in this case, which occurs at the interface composite-penetrant. Second one is diffusion through the solid composite. Therefore the permeation coefficient *P*, that includes the two previous phenomena, is the transport rate of diffusants to penetrate through the material's thickness under specified temperature and humidity conditions. It can be determined by combining the diffusion coefficient *D* and sorption coefficient *S* by Equation 1.10 obtaining the values shown in Table 3.4.

Table 3.4. Permeation coefficient *P* for all hydrothermal condition and amount of fiber.

P ·10^9 (cm^{2}s^{-1})	**Hydrothermal condition (ºC)**											
	60		**65**		**70**		**75**		**80**		**85**	
Fiber content (%f)	**Coupling agent**											
	Yes	**No**	**Yes**	**No**	**Yes**	**No**	**Yes**	**No**	**Yes**	**No**	**Yes**	**No**
0	1,9 (±0,1)		2,1 (±0,1)		3,2 (±0,0)		8,9 (±0,2)		10,4 (±0,4)		10,0 (±0,3)	
10	5,3 (±0,2)	6,6 (±0,3)	4,2 (±0,1)	9,5 (±0,4)	5,9 (±0,1)	10,8 (±0,2)	9,2 (±0,2)	9,2 (±0,3)	4,1 (±0,1)	12,3 (±0,5)	15,9 (±0,5)	16,5 (±0,8)
20	7,3 (±0,2)	12,1 (±0,4)	10,4 (±0,3)	13,7 (±0,5)	10,7 (±0,3)	20,4 (±1,0)	13,7 (±0,4)	16,1 (±0,7)	17,5 (±0,6)	22,0 (±0,6)	20,0 (±0,7)	25,7 (±1,0)
30	18,7 (±0,4)	22,4 (±0,6)	19,7 (±0,4)	21,5 (±0,6)	21,7 (±0,9)	36,0 (±1,4)	22,5 (±1,0)	28,4 (±1,3)	27,2 (±0,9)	29,1 (±1,0)	32,6 (±1,2)	32,5 (±0,9)

Permeation coefficient shows tendencies combined from both parameters it involves. On the one hand, as well as for the diffusion coefficient, *P* exhibits the same temperature dependence, growing when temperature is increased. On the other hand, permeation coefficient is higher for composites with high amount of fiber. This tendency is determined in this case by sorption coefficient.

Broadly speaking, permeation is greater for high temperatures and high amount of sisal fiber.

As a mode of summary of this section, the influence of the experiment variables on each other, are represented in an interaction plot in Figure 3.5. Results about saturation water mas M_s and diffusion coefficient *D* are represented for combination of two of the variables under study (temperature, fiber and coupling agent) giving an overall picture.

In the right-superior part of the Figure 3.5 (graphs d, e and f) it can be appreciated that M_s-mean was not affected by temperature for different amounts of fiber (e) and presence of coupling agent (f). M_s-mean was slightly modified by the presence of coupling agent for composites, but not in a clear tendency (d).

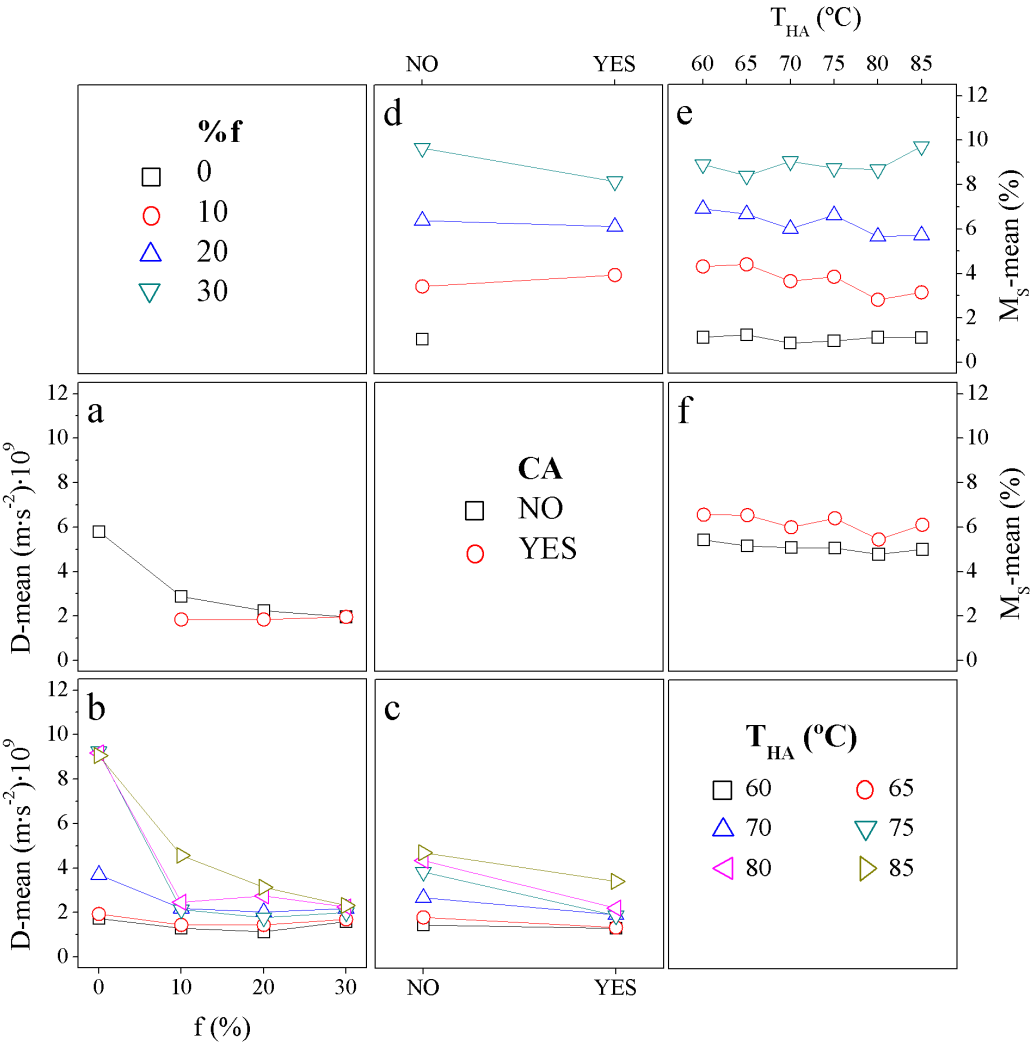

Figure 3.5. Interaction plot of M_s and *D*-means versus amount of fiber, coupling agent and temperature.

The left-inferior part shows *D*-means for different factors combinations (graphs a, b and c). From (a) graph, it can be observed that *D* was higher for VPLA than for composites, presenting similar values for presence or not of coupling agent. From (c) graph it can be appreciated that presence of coupling agent slightly decreased *D* for all temperatures. Finally, at different temperatures, in graph (b), it can be seen that higher temperatures resulted in a higher *D*, much more for VPLA than for composites. As higher is fiber content, similar values were obtained for high temperatures, being even the same for PLA30/30C for all hydrothermal conditions. It suggested a change in composite structure, as commented before.

The presence of water into the polymer matrices and temperature effect could be a cause of microstructure change and modification of the final properties of the material. Plasticization of the amorphous portion, crystallistion and/or hydrolytic chain scission reactions that can promote a change on internal material structure was thus approached by thermal analysis.

3.3 Thermal behaviour

The degradation of composites with PLA semi-crystalline matrices proceeds in a complicated way. Fischer et al. [50] reported that hydrothermal degradation proceeds in two stages. During the first stage, water diffuses into the amorphous regions, resulting in random hydrolytic scission of ester bonds. The degree of crystallinity can even increase as degradation proceeds. The second stage starts after degradation of the major part of the amorphous area. The hydrolytic attack proceeds from the edge towards the centre of crystalline domains. Degradation becomes a bulk process above T_g, as in this case, while at temperatures below T_g degradation of the polymer matrix is restricted to its surface [51].

In order to approach this degradation process, thermo-gravimetric analysis and differential scanning calorimetry assays were carried out.

3.3.1 Thermo-Gravimetric analysis (TGA)

The purpose of this analysis was to ascertain the state of chemical degradation in the composite and in case it was, how important had been it. Accordingly, it was analysed materials before and after being exposed to hydrothermal degrading conditions, as well sisal fiber and PLA matrix separately.

Resulting thermogram for sisal fiber decomposition shows four different regions (Figure 3.6). The TG curve of raw sisal showed a weight loss of 8.5 % in the temperature range of 25-194 ºC which is due to the loss of absorbed water in the fiber (intra- and intermolecular dehydration reactions) [54].

Sisal fiber degradation started at about 195 ºC and proceeded very fast with temperature increase, showing a weight loss of 62.7 % in the range of 195-360 ºC. The weight losses at temperature ranges of 195-314 ºC and 314-360 ºC were 26.5 and 36.2%, respectively. These results are an indication of a fast rate of fiber degradation that started at 195 ºC and became faster at 314 ºC. This behaviour was shown by a slope change at 314 ºC.

The derivative thermogram curve (DTG) for sisal fiber showed two distinct peaks. Each peak gave the temperature where degradation is faster for each step. In this case, two peaks at 289 and 325 ºC indicated that the degradation of sisal fiber occurs in two steps. This first peak was a shoulder on the main degradation peak, attributed to the hemicellulose degradation. Thermal degradation of cellulose occurs at higher temperatures compared with hemicellulose and at a

faster degradation rate. The main degradation peak started about 314 ºC and was completed at 360 ºC with a maximum at 325 ºC. All these results are according with other studies [55].

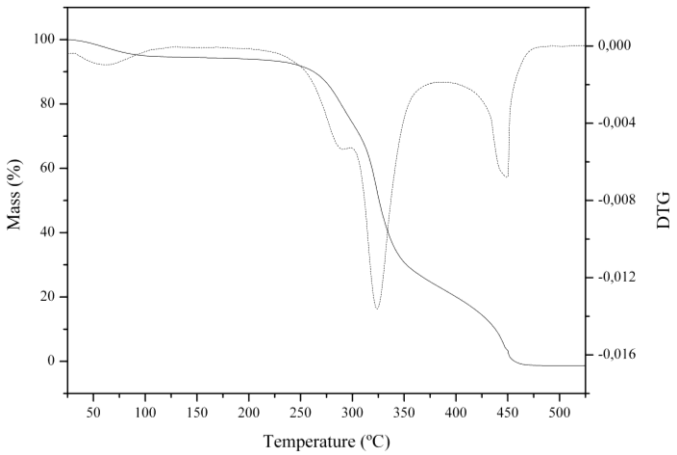

Figure 3.6. TG and DTG of untreated sisal fiber.

Figure 3.7 contains TG curve for non-degraded matrix (VPLA) and showed a one-stage decomposition in the range of 280-380 ºC and subsequent char decomposition from 380 to 500 ºC. From DTG curves, it can be obtained temperature in which degradation is faster; in this case, around 356 ºC.

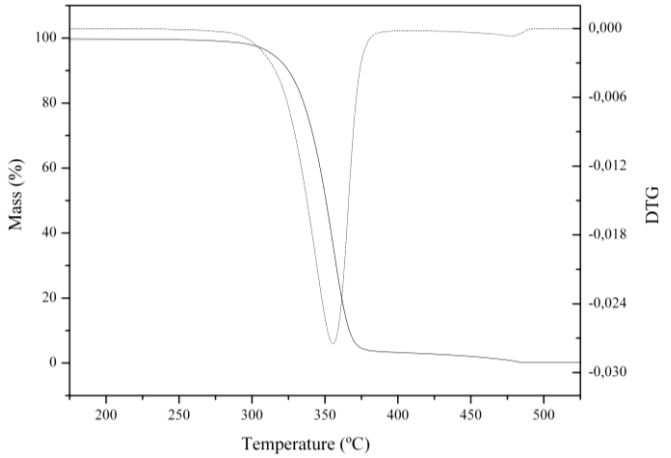

Figure 3.7. PLA TG and DTG curves.

Once sisal fiber and PLA matrix have been analysed separately, sisal fiber composites can be properly approached. TG curves for composites showed four regions as sisal fiber did. First initial loss is related with water present in both the matrix and fiber. Second weight loss region, in the range of 222-315 ºC, is due to the degradation of hemicellulose. Third weight loss, in the range of 315-400 ºC, is caused by degradation of both the polymer matrix and

cellulose, which peaks are overlapped. Final weight loss, as in fiber and matrix case, is due to the degradation of char formed during decomposition.

The discussion is given in terms of onset degradation temperature (T_o) and main degradation process temperature (T_{md}).

Onset degradation temperature (T_0) decreased as amount of fiber increased in composites. It has been calculated as temperature in which mass loss was 5%. This decrement is due to the incorporation of the sisal fiber into the polymer matrix which has a lower onset temperature.

Even though, onset temperature for composites was higher than for sisal fiber, increment attributed to a kind of protection of fiber by polymer matrix, according to Albano et al. [56].

Figure 3.8, 3.9 and 3.10 shows TG curves for all materials and hydrothermal conditions andFigure 3. values of onset temperature can be found on Table 3.5.

Table 3.5. Onset temperature for all hydrothermal conditions.

T_0 (ºC)	**Non degraded**		**Hydrothermal condition (ºC)**					
			65		**75**		**85**	
Fiber content (%f)	**Coupling agent**							
	Yes	**No**	**Yes**	**No**	**Yes**	**No**	**Yes**	**No**
0	313,8 (±0,2)		307,2 (±0,4)		307,3 (±0,2)		307,1 (±0,2)	
10	299,7 (±0,3)	313,4 (±0,4)	301,7 (±0,6)	312,8 (±1,1)	309,5 (±0,6)	313,9 (±0,9)	313,6 (±0,0)	311,1 (±0,7)
20	283,3 (±0,2)	303,9 (±0,1)	292,3 (±0,8)	302,7 (±0,5)	294,7 (±1,1)	297,4 (±0,6)	288,9 (±0,5)	288,3 (±0,1)
30	273,1 (±0,3)	285,2 (±0,1)	284,9 (±0,0)	289,2 (±0,5)	282,4 (±1,0)	285,9 (±0,6)	290,6 (±0,2)	285,4 (±0,2)

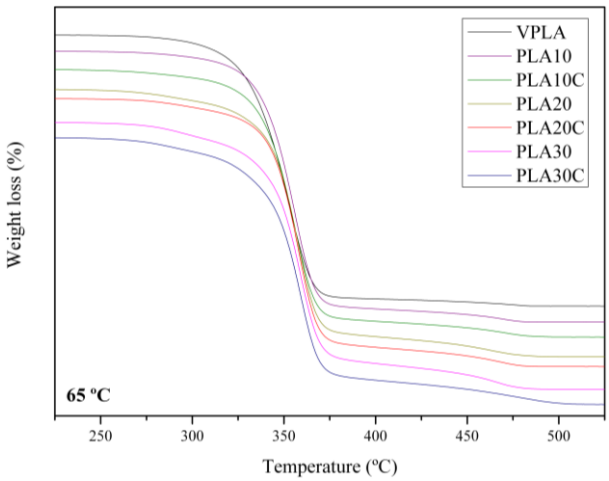

Figure 3.8. TG curves for VPLA and composites for 65 ºC hydrothermal condition.

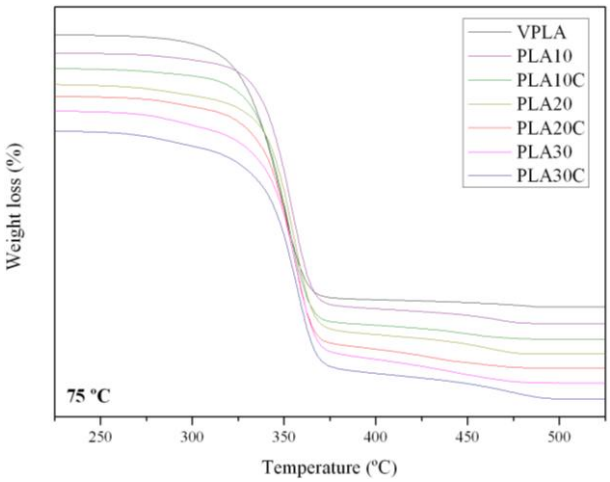

Figure 3.9. TG curves for VPLA and composites for 75 ºC hydrothermal condition.

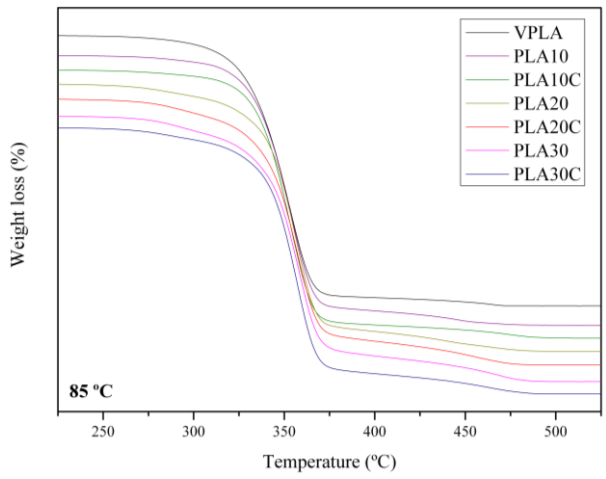

Figure 3.10. TG curves for VPLA and composites for 85 ºC hydrothermal condition.

Moreover, the main degradation process temperature (T_{md}) was assessed too. Higher values were obtained when sisal fiber content was increased in biocomposites.Values for T_{md} were in the range between 350 for VPLA and 359 ºC for PLA30/30C. Both samples, with and without coupling agent had similar results and there was not a significant change for different hydrothermal conditions. The increment on main degradation temperature may be due to a synergic effect of fiber and matrix. T_{md} values are shown in Table 3.6 and tendencies can be observed in Figure 3.11, 3.12 and 3.13.

Table 3.6. Main degradation temperature for all hydrothermal conditions.

T_{md} (ºC)	**Non degraded**		**Hydrothermal condition (ºC)**					
			65		**75**		**85**	
Fiber content (%f)	**Coupling agent**							
	Yes	**No**	**Yes**	**No**	**Yes**	**No**	**Yes**	**No**
0	355,9 (±0,3)		352,1 (±0,5)		350,5 (±0,1)		350,1 (±2,8)	
10	352,6 (±0,5)	353,4 (±0,4)	354,2 (±0,7)	355,6 (±1,0)	353,5 (±0,7)	355,4 (±0,2)	352,5 (±1,0)	352,2 (±0,9)
20	356,9 (±0,5)	355,2 (±0,0)	358,7 (±0,9)	356,6 (±0,4)	353,2 (±3,1)	354,8 (±0,6)	357,1 (±0,0)	355,4 (±1,1)
30	354,2 (±0,4)	353,4 (±0,1)	359,7 (±0,1)	358,0 (±0,3)	356,4 (±1,7)	356,8 (±0,2)	357,7 (±0,2)	357,8 (±0,3)

In summary, non-significant differences could be appreciated between thermograms of composites, matrix and fiber. Composites behaviour in TGA is like an addition of both thermograms VPLA and sisal fiber. This tendency is the same for non-degraded samples and degraded ones.

At this point we can say that degradation did not affect on a massive scale to the chemical structure. Physical ageing seem to be the most important effect of hydrothermal treatment. In next section, physical structure and changes will be approached by means of Differential Scanning Calorimetry (DSC).

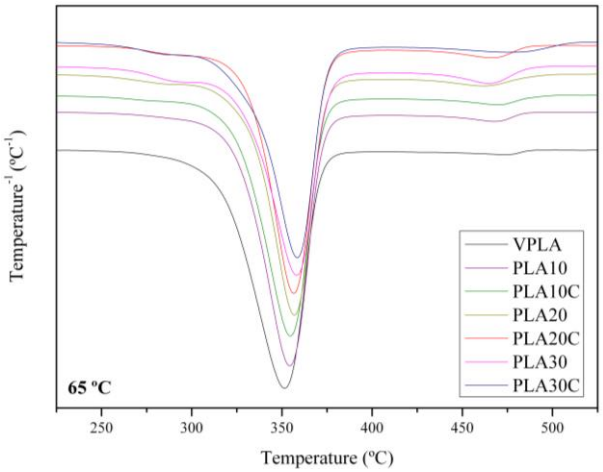

Figure 3.11. DTG curves for VPLA and composites 65 ºC hydrothermal condition.

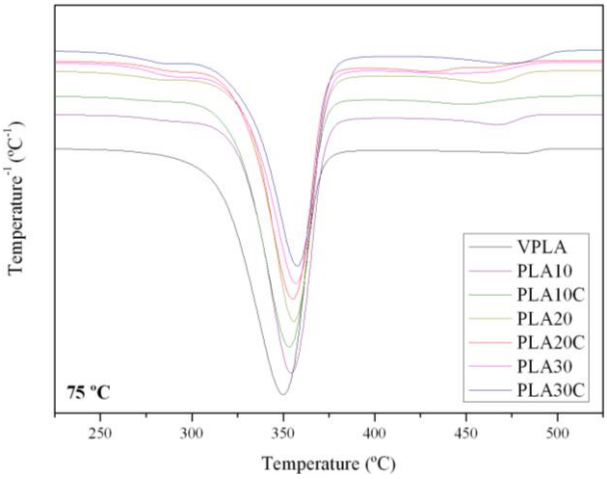

Figure 3.12. DTG curves for VPLA and composites for 75 ºC hydrothermal condition.

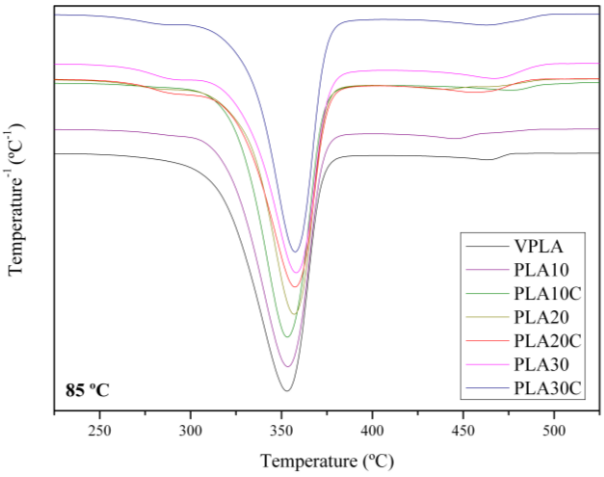

Figure 3.13. DTG curves for VPLA and composites for 85 ºC hydrothermal condition.

3.3.2 Differential Scanning Calorimetry (DSC)

The hydrodegradation process was monitored in order to evaluate effects of hydrothermal degrading conditions along the water absorption process. By this technique, samples were analysed for different times during the assay for a given temperature and a given material, so the material could be analytically characterized along the whole process of swelling. These times of water absorption assay were established at 0, 25, 50 and 100% of the saturation mass (M_s). Thus, extraction times were different for each material and temperature, but at the same percentage of water uptake.

The PLA relaxation associated to the glass transition (gt-r), followed by polymer cold crystallization (cc_1 and cc_2) and polymer melting (m) could be observed on thermograms for all samples at the first heating scan. These three thermal events are typical for semi-crystalline PLA based composites [54]. Similar curve could be seen on second heating ramp. On cooling scan, there was a cristallisation, followed by a glass transition phenomena. All these events can be observed at Figure 3.14, gived as a example.

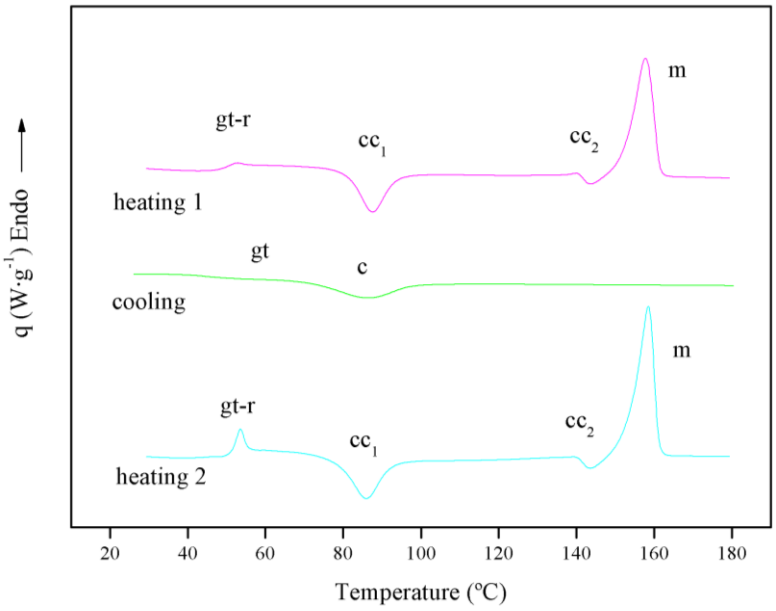

Figure 3.14. Example of events at first and second heating scan as well as cooling ramp.

Process monitoring thermograms of the first heating scan in Figure 3.15 and calorimetric data can be found in Table 3.7, 3.8 and 3.9.

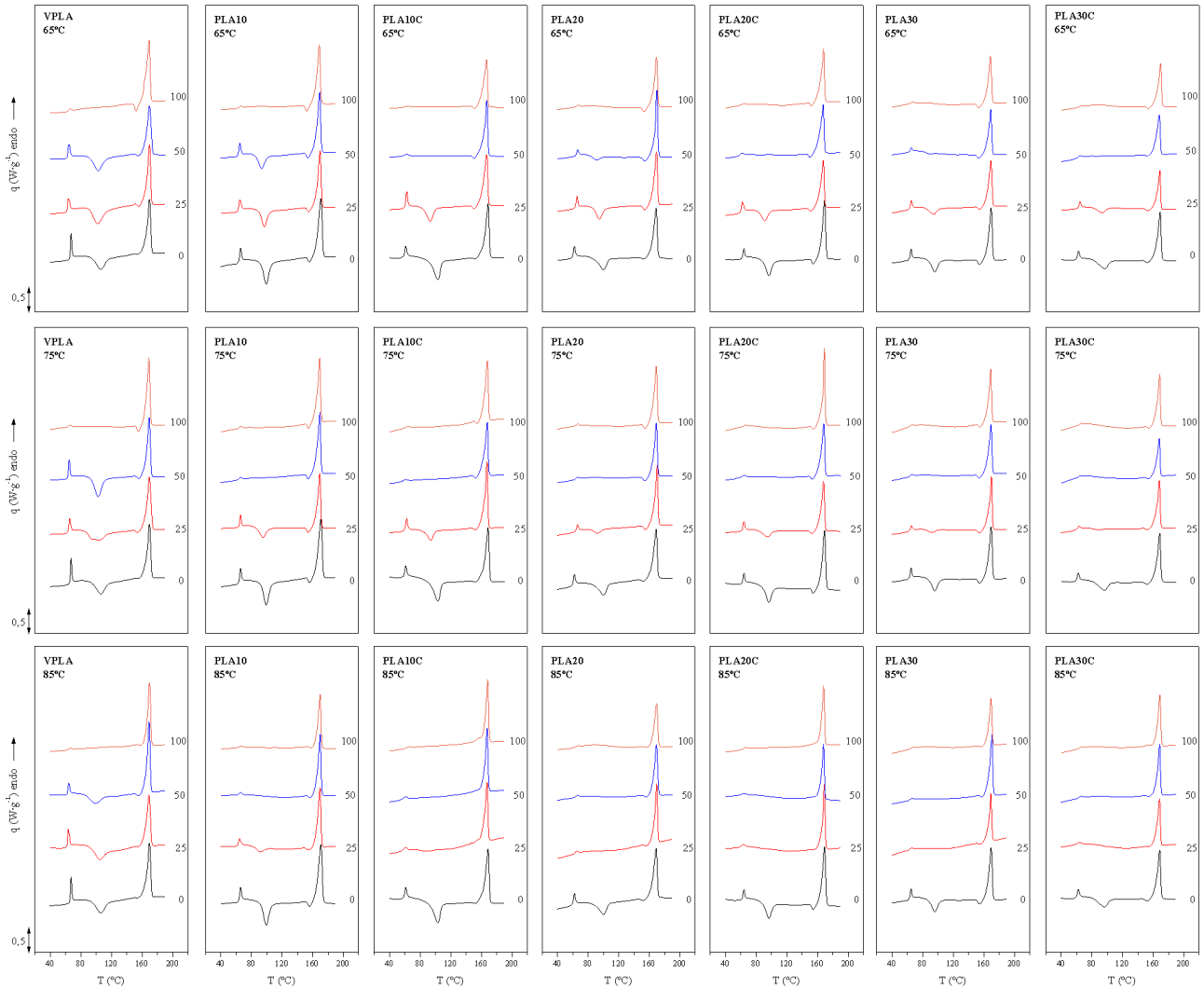

Figure 3.15. First heating scan for PLA and composites for different hydrothermal condition (65, 75 and 85 ºC) and saturation degrees (0, 25, 50 and 100%).

Table 3.7. First heating scan data for PLA and composites at 65 ºC and different saturation degrees.

65 ºC	Sat (%)	ΔH_{gt} (J/g)		$T_{g\text{-}p}$ (ºC)		ΔH_{cc1} (J/g)		T_{cc1} (ºC)		ΔH_{cc2} (J/g)		T_{cc2} (ºC)		ΔH_m (J/g)		T_m (ºC)		Xc (%)	
VPLA	**0**	5,9	(±0,1)	66,9	(±0,2)	-19,4	(±1,2)	105,1	(±0,3)	-	-	-	-	35,5	(±0,8)	169,2	(±0,1)	17,3	(±1,6)
	25	5,8	(±0,1)	64,3	(±0,5)	-19,7	(±0,5)	103,8	(±1,4)	-0,7	(±0,3)	155,4	(±0,1)	37,1	(±1,1)	169,9	(±0,4)	17,9	(±5,9)
	50	5,5	(±0,2)	63,0	(±1,6)	-21,3	(±1,3)	102,0	(±0,3)	-1,0	(±0,2)	154,8	(±0,1)	40,5	(±2,2)	169,3	(±0,1)	19,6	(±11,7)
	100	0,8	(±0,1)	65,9	(±0,1)	-	-	-	-	-4,0	(±0,2)	151,7	(±0,2)	43,1	(±1,5)	168,8	(±0,2)	42,0	(±3,4)
PLA10	**0**	4,4	(±0,4)	66,8	(±0,1)	-17,3	(±1,9)	98,0	(±0,3)	-1,7	(±0,2)	154,9	(±0,2)	33,8	(±2,6)	169,0	(±0,1)	17,7	(±5,1)
	25	4,2	(±0,0)	64,8	(±0,1)	-15,8	(±0,5)	96,7	(±0,2)	-2,0	(±0,1)	154,8	(±0,2)	37,7	(±1,0)	169,5	(±0,2)	23,8	(±1,2)
	50	4,0	(±0,1)	64,9	(±0,2)	-12,7	(±0,4)	93,7	(±0,3)	-2,4	(±0,1)	153,4	(±0,1)	38,5	(±1,1)	168,9	(±0,1)	27,9	(±1,0)
	100	0,8	(±0,1)	66,2	(±0,1)	-	-	-	-	-3,1	(±0,1)	152,2	(±0,1)	39,4	(±0,1)	168,5	(±0,2)	43,3	(±0,6)
PLA10C	**0**	6,2	(±0,1)	62,8	(±0,2)	-21,7	(±0,5)	98,9	(±0,5)	-	-	-	-	35,5	(±1,3)	166,9	(±0,3)	16,9	(±1,0)
	25	4,7	(±0,5)	62,9	(±0,4)	-15,7	(±0,6)	93,7	(±0,4)	-1,7	(±0,1)	150,7	(±0,4)	36,9	(±1,9)	167,0	(±0,2)	23,9	(±2,7)
	50	0,8	(±0,1)	61,6	(±0,2)	-	-	-	-	-1,3	(±0,1)	149,9	(±0,3)	35,4	(±1,1)	166,5	(±0,1)	41,6	(±3,6)
	100	0,4	(±0,1)	63,4	(±0,2)	-	-	-	-	-0,9	(±0,1)	150,9	(±0,1)	37,5	(±2,8)	166,4	(±0,2)	44,6	(±4,1)
PLA20	**0**	4,2	(±0,3)	67,2	(±0,1)	-15,8	(±0,6)	96,3	(±0,1)	-2,0	(±0,3)	154,1	(±0,3)	33,4	(±0,9)	168,9	(±0,1)	21,4	(±1,1)
	25	3,4	(±0,1)	65,4	(±0,2)	-12,2	(±0,9)	94,3	(±0,2)	-2,5	(±0,1)	154,0	(±0,1)	32,5	(±0,7)	169,1	(±0,2)	24,5	(±2,9)
	50	1,9	(±0,2)	65,8	(±0,3)	-4,1	(±0,2)	90,6	(±0,2)	-2,0	(±0,4)	153,5	(±0,5)	33,5	(±0,2)	169,1	(±0,3)	37,7	(±1,3)
	100	0,7	(±0,1)	67,1	(±0,1)	-	-	-	-	-2,5	(±0,1)	153,0	(±0,1)	33,0	(±0,9)	169,1	(±0,2)	42,0	(±1,8)
PLA20C	**0**	2,1	(±0,5)	67,7	(±0,2)	-6,5	(±0,4)	95,3	(±0,1)	-1,5	(±0,1)	154,2	(±0,1)	27,8	(±0,4)	169,2	(±0,1)	26,6	(±1,2)
	25	4,3	(±0,1)	62,4	(±0,3)	-11,8	(±0,1)	92,0	(±0,7)	-1,2	(±0,3)	151,7	(±0,3)	33,3	(±0,7)	167,6	(±0,1)	27,3	(±0,5)
	50	1,7	(±0,1)	60,9	(±0,3)	-	-	-	-	-1,4	(±0,1)	150,0	(±0,1)	36,0	(±0,5)	166,7	(±0,4)	46,4	(±1,6)
	100	0,8	(±0,1)	65,0	(±0,3)	-	-	-	-	-1,5	(±0,2)	151,7	(±0,2)	34,5	(±0,3)	167,8	(±0,1)	44,4	(±0,2)
PLA30	**0**	2,5	(±0,4)	67,6	(±0,1)	-6,5	(±2,9)	95,3	(±0,8)	-1,5	(±0,3)	154,2	(±0,2)	27,8	(±1,3)	169,2	(±0,2)	30,4	(±2,0)
	25	2,2	(±0,1)	65,7	(±0,1)	-7,7	(±0,5)	94,6	(±0,1)	-1,7	(±0,1)	154,0	(±0,1)	29,5	(±0,3)	169,1	(±0,1)	30,8	(±0,5)
	50	1,4	(±0,1)	65,5	(±0,1)	-	-	-	-	-2,0	(±0,1)	153,3	(±0,1)	28,8	(±0,2)	169,0	(±0,2)	41,1	(±1,5)
	100	0,4	(±0,1)	67,2	(±0,1)	-	-	-	-	-1,5	(±0,1)	153,5	(±0,1)	32,5	(±0,9)	168,9	(±0,3)	47,6	(±1,7)
PLA30C	**0**	3,2	(±0,1)	65,6	(±0,5)	-9,8	(±0,2)	93,3	(±0,7)	-1,0	(±0,1)	152,8	(±0,4)	29,3	(±0,3)	168,1	(±0,4)	29,2	(±0,6)
	25	2,6	(±0,2)	63,4	(±0,8)	-6,0	(±0,2)	91,5	(±1,5)	-0,8	(±0,1)	151,9	(±0,3)	25,4	(±1,5)	167,7	(±0,5)	29,5	(±2,8)
	50	1,7	(±0,1)	60,9	(±0,3)	-	-	-	-	-0,7	(±0,1)	151,4	(±0,1)	28,1	(±0,3)	167,3	(±0,1)	43,4	(±0,4)
	100	0,3	(±0,1)	65,0	(±0,3)	-	-	-	-	-0,9	(±0,2)	152,9	(±0,2)	28,4	(±0,2)	168,6	(±0,7)	43,4	(±1,5)

Table 3.8. First heating scan data for PLA and composites at 75 ºC and different saturation degrees.

75 ºC	Sat (%)	ΔH_{gt} (J/g)		$T_{g\text{-}p}$ (ºC)		ΔH_{cc1} (J/g)		T_{cc1} (ºC)		ΔH_{cc2} (J/g)		T_{cc2} (ºC)		ΔH_m (J/g)		T_m (ºC)		Xc (%)	
VPLA	**0**	5,9	(±0,1)	66,9	(±0,2)	-19,4	(±1,2)	105,1	(±0,3)	-	-	-	-	35,5	(±0,8)	169,2	(±0,1)	17,3	(±2,1)
	25	4,3	(±0,4)	65,8	(±0,4)	-16,9	(±2,8)	104,9	(±2,4)	-0,7	(±0,4)	153,8	(±0,3)	35,9	(±4,0)	169,8	(±0,7)	19,6	(±7,8)
	50	4,4	(±0,1)	64,8	(±0,1)	-19,2	(±4,8)	103,2	(±0,3)	-0,8	(±0,1)	155,3	(±0,1)	37,2	(±0,5)	168,9	(±0,2)	18,4	(±5,7)
	100	1,0	(±0,1)	66,0	(±0,1)	-	-	-	-	-2,6	(±0,3)	154,4	(±0,3)	41,2	(±1,0)	168,4	(±0,1)	41,4	(±1,3)
PLA10	**0**	4,4	(±0,4)	66,8	(±0,1)	-17,3	(±1,9)	98,0	(±0,3)	-1,7	(±0,2)	154,9	(±0,2)	33,8	(±2,6)	169,0	(±0,1)	17,7	(±5,6)
	25	3,0	(±0,1)	65,6	(±0,1)	-12,2	(±1,0)	95,6	(±0,6)	-2,5	(±0,1)	154,2	(±0,1)	35,5	(±2,4)	169,3	(±0,3)	24,8	(±4,1)
	50	1,1	(±0,1)	65,9	(±0,3)	-	-	-	-	-1,9	(±0,1)	154,5	(±0,4)	39,0	(±0,4)	169,9	(±0,8)	44,3	(±0,5)
	100	0,8	(±0,1)	66,0	(±0,1)	-	-	-	-	-2,4	(±0,1)	154,4	(±0,3)	39,5	(±0,6)	169,0	(±0,1)	44,3	(±0,8)
PLA10C	**0**	6,2	(±0,1)	62,8	(±0,2)	-21,7	(±0,5)	98,9	(±0,5)	-	-	-	-	35,5	(±1,3)	166,9	(±0,3)	16,9	(±2,2)
	25	4,6	(±0,1)	61,8	(±0,5)	-10,7	(±0,2)	92,8	(±1,0)	-0,9	(±0,2)	151,8	(±0,3)	36,8	(±2,5)	166,5	(±0,3)	30,8	(±3,5)
	50	0,6	(±0,1)	60,1	(±1,0)	-	-	-	-	-0,7	(±0,2)	151,8	(±0,5)	34,6	(±1,2)	166,4	(±1,1)	41,4	(±1,7)
	100	0,6	(±0,1)	64,4	(±0,2)	-	-	-	-	-0,7	(±0,1)	154,0	(±0,1)	37,5	(±2,1)	167,4	(±0,1)	45,0	(±2,6)
PLA20	**0**	4,2	(±0,3)	67,2	(±0,1)	-15,8	(±0,6)	96,3	(±0,1)	-2,0	(±0,3)	154,1	(±0,3)	33,4	(±0,9)	168,9	(±0,1)	21,4	(±2,4)
	25	1,9	(±0,1)	65,6	(±0,3)	-4,2	(±0,5)	92,1	(±0,2)	-2,0	(±0,1)	154,4	(±0,2)	32,7	(±1,7)	169,5	(±0,3)	36,6	(±3,2)
	50	0,7	(±0,1)	66,3	(±0,1)	-	-	-	-	-1,9	(±0,1)	154,0	(±0,1)	34,3	(±0,7)	169,1	(±0,1)	44,6	(±1,0)
	100	0,7	(±0,1)	66,5	(±0,3)	-	-	-	-	-1,4	(±0,3)	154,2	(±0,3)	35,2	(±1,4)	169,4	(±0,6)	46,6	(±2,3)
PLA20C	**0**	2,1	(±0,5)	67,7	(±0,2)	-6,5	(±0,4)	95,3	(±0,1)	-1,5	(±0,1)	154,2	(±0,1)	27,8	(±0,4)	169,2	(±0,1)	26,6	(±1,2)
	25	3,1	(±0,1)	63,6	(±0,5)	-7,7	(±0,7)	94,1	(±0,8)	-1,1	(±0,1)	152,5	(±0,1)	32,9	(±0,3)	167,8	(±0,1)	32,5	(±1,3)
	50	0,8	(±0,1)	64,3	(±0,2)	-	-	-	-	-1,7	(±0,1)	153,3	(±0,2)	33,0	(±1,7)	168,0	(±0,1)	42,0	(±2,3)
	100	0,4	(±0,1)	66,6	(±0,2)	-	-	-	-	-1,7	(±0,1)	155,0	(±0,3)	35,6	(±0,7)	169,2	(±0,6)	45,5	(±0,9)
PLA30	**0**	2,5	(±0,4)	67,6	(±0,1)	-6,5	(±2,9)	95,3	(±0,8)	-1,5	(±0,3)	154,2	(±0,2)	27,8	(±1,3)	169,2	(±0,2)	30,4	(±6,9)
	25	1,0	(±0,4)	65,1	(±0,3)	-3,6	(±0,6)	91,5	(±0,4)	-1,8	(±0,1)	154,0	(±0,2)	31,0	(±2,0)	168,9	(±0,7)	39,3	(±4,2)
	50	0,4	(±0,1)	66,0	(±0,1)	-	-	-	-	-1,7	(±0,2)	153,9	(±0,4)	31,1	(±0,1)	169,0	(±0,6)	45,2	(±0,5)
	100	0,3	(±0,1)	66,5	(±0,1)	-	-	-	-	-1,5	(±0,2)	154,6	(±0,1)	31,4	(±0,3)	168,5	(±0,1)	45,9	(±0,7)
PLA30C	**0**	3,2	(±0,1)	65,6	(±0,5)	-9,8	(±0,2)	93,3	(±0,7)	-1,0	(±0,1)	152,8	(±0,4)	29,3	(±0,3)	168,1	(±0,4)	29,2	(±0,8)
	25	1,4	(±0,1)	63,4	(±0,2)	-1,9	(±0,2)	89,8	(±1,0)	-1,0	(±0,1)	153,0	(±0,1)	29,3	(±0,3)	168,1	(±0,1)	41,7	(±1,1)
	50	0,4	(±0,1)	64,3	(±0,4)	-	-	-	-	-0,9	(±0,3)	153,7	(±0,1)	27,4	(±0,9)	167,7	(±0,3)	41,8	(±1,9)
	100	0,3	(±0,1)	65,9	(±0,1)	-	-	-	-	-0,7	(±0,1)	154,1	(±0,1)	29,1	(±1,6)	167,9	(±0,4)	44,9	(±2,6)

Table 3.9. First heating scan data for PLA and composites at 85 ºC and different saturation degrees.

85 ºC	Sat (%)	ΔH_{gt} (J/g)		$T_{g\text{-}p}$ (ºC)		ΔH_{cc1} (J/g)		T_{cc1} (ºC)		ΔH_{cc2} (J/g)		T_{cc2} (ºC)		ΔH_m (J/g)		T_m (ºC)		Xc (%)	
VPLA	**0**	5,9	(±0,1)	66,9	(±0,2)	-19,4	(±1,2)	105,1	(±0,3)	-	-	-	-	35,5	(±0,8)	169,2	(±0,1)	17,3	(±2,1)
	25	4,8	(±0,8)	63,8	(±0,1)	-21,4	(±0,5)	103,4	(±1,2)	-0,6	(±0,2)	155,3	(±0,1)	35,8	(±1,1)	168,9	(±0,3)	14,8	(±2,0)
	50	2,6	(±0,6)	64,2	(±0,1)	-9,3	(±5,4)	96,2	(±2,9)	-1,8	(±0,7)	154,9	(±0,2)	38,9	(±2,4)	168,8	(±0,1)	29,9	(±9,0)
	100	0,8	(±0,1)	66,1	(±0,1)	-	-	-	-	-	-	-	-	35,9	(±0,1)	169,5	(±0,2)	38,5	(±0,0)
PLA10	**0**	4,4	(±0,4)	66,8	(±0,0)	-17,3	(±1,9)	98,0	(±0,3)	-1,7	(±0,2)	154,9	(±0,2)	33,8	(±2,6)	169,0	(±0,1)	17,7	(±5,6)
	25	3,1	(±0,3)	64,3	(±0,1)	-8,4	(±1,4)	91,8	(±0,3)	-1,8	(±0,1)	154,4	(±0,2)	35,9	(±0,1)	169,4	(±0,2)	30,6	(±1,8)
	50	0,8	(±0,0)	65,8	(±0,1)	-	-	-	-	-0,8	(±0,1)	156,0	(±0,0)	34,8	(±0,9)	169,2	(±0,1)	40,5	(±1,2)
	100	0,8	(±0,1)	66,3	(±0,2)	-	-	-	-	-0,9	(±0,3)	157,2	(±0,5)	35,9	(±2,3)	169,5	(±0,1)	41,7	(±3,1)
PLA10C	**0**	6,2	(±0,1)	62,8	(±0,2)	-21,7	(±0,5)	98,9	(±0,5)	-	-	-	-	35,5	(±1,3)	166,9	(±0,3)	16,9	(±2,2)
	25	1,3	(±0,4)	60,5	(±0,1)	-3,7	(±1,5)	89,7	(±0,1)	-	-	-	-	36,3	(±0,7)	167,1	(±0,1)	39,8	(±2,7)
	50	0,7	(±0,1)	60,4	(±0,5)	-	-	-	-	-	-	-	-	35,5	(±3,6)	167,1	(±0,0)	43,3	(±4,4)
	100	0,5	(±0,1)	65,2	(±0,1)	-	-	-	-	-	-	-	-	38,2	(±0,8)	167,9	(±0,3)	46,7	(±1,0)
PLA20	**0**	4,2	(±0,3)	67,2	(±0,1)	-15,8	(±0,6)	96,3	(±0,1)	-2,0	(±0,3)	154,1	(±0,3)	33,4	(±0,9)	168,9	(±0,1)	21,4	(±2,4)
	25	0,9	(±0,1)	65,3	(±0,1)	-	-	-	-	-0,6	(±0,1)	156,1	(±0,1)	30,0	(±1,1)	169,2	(±0,1)	40,6	(±1,6)
	50	0,6	(±0,1)	66,0	(±0,1)	-	-	-	-	-0,9	(±0,1)	155,8	(±0,2)	31,3	(±0,7)	169,1	(±0,3)	41,9	(±1,1)
	100	0,3	(±0,0)	66,9	(±0,1)	-	-	-	-	-0,6	(±0,1)	156,6	(±0,1)	32,6	(±0,8)	169,4	(±0,1)	44,0	(±1,2)
PLA20C	**0**	2,1	(±0,5)	67,7	(±0,2)	-6,5	(±0,4)	95,3	(±0,1)	-1,5	(±0,1)	154,2	(±0,1)	27,8	(±0,4)	169,2	(±0,1)	26,6	(±1,2)
	25	0,8	(±0,2)	62,1	(±0,7)	-	-	-	-	-	-	-	-	32,5	(±0,8)	168,4	(±0,5)	43,6	(±1,0)
	50	1,1	(±0,1)	64,6	(±0,1)	-	-	-	-	-	-	-	-	34,1	(±1,2)	167,8	(±0,2)	45,7	(±1,7)
	100	0,2	(±0,1)	65,9	(±0,2)	-	-	-	-	-	-	-	-	32,4	(±1,2)	168,2	(±0,3)	43,5	(±1,6)
PLA30	**0**	2,5	(±0,4)	67,6	(±0,1)	-6,5	(±2,9)	95,3	(±0,8)	-1,5	(±0,3)	154,2	(±0,2)	27,8	(±1,3)	169,2	(±0,2)	30,4	(±6,9)
	25	0,6	(±0,1)	65,3	(±0,4)	-	-	-	-	-0,5	(±0,1)	155,0	(±0,2)	27,9	(±2,4)	169,0	(±0,1)	42,1	(±3,9)
	50	0,6	(±0,1)	66,0	(±0,3)	-	-	-	-	-0,6	(±0,1)	156,6	(±0,5)	34,4	(±0,3)	169,6	(±0,9)	51,8	(±0,6)
	100	0,3	(±0,1)	67,0	(±0,1)	-	-	-	-	-0,8	(±0,1)	156,8	(±0,1)	36,8	(±1,2)	169,4	(±0,1)	55,2	(±1,9)
PLA30C	**0**	3,2	(±0,0)	65,6	(±0,5)	-9,8	(±0,2)	93,3	(±0,7)	-1,0	(±0,1)	152,8	(±0,4)	29,3	(±0,3)	168,1	(±0,4)	29,2	(±0,8)
	25	0,8	(±0,1)	62,9	(±0,5)	-	-	-	-	-	-	-	-	28,8	(±0,1)	167,7	(±0,7)	45,5	(±0,1)
	50	0,5	(±0,1)	65,6	(±0,2)	-	-	-	-	-0,3	(±0,2)	154,0	(±0,4)	27,5	(±1,5)	168,1	(±0,4)	42,9	(±2,3)
	100	0,3	(±0,1)	66,3	(±0,2)	-	-	-	-	-	-	-	-	30,8	(±0,5)	168,6	(±0,1)	48,7	(±0,9)

Enthalpy associated to the glass transition (ΔH_{gt}) and its associated temperature peak ($T_{g\text{-}P}$) was evaluated first. This structural relaxation enthalpy, associated to the physical ageing process, decreased along the absorption process for all cases, reaching lower values for composites with less polymeric phase. This decrease of $T_{g\text{-}P}$ was faster for high temperatures than for lower ones, due to the kinetic effect, indicating the plasticizing effect of water on the polymer matrix [46]. Plasticizing effect was much important as water absorption increased.

With regards to cold-crystallization phenomenon, its enthalpy (ΔH_{cc1}) and its peak temperature (T_{cc1}) were evaluated too. T_{cc1} was generally displaced to lower temperatures (1-7 ºC) when sample saturation increased. In general, composites showed lower cold crystallisation temperatures. ΔH_{cc1} changed along the water absorption process showing a decrease and, in most cases, disappearing for the last water absorption stages (50 and 100%). This disappearance occurred earlier for high temperatures. In composites, the disappearance was earlier than for VPLA and values were lower when fiber content increased. It indicates that the most part of amorphous material had already crystallised during water absorption experiment. This phenomenon is accelerated by fiber and hydrothermal condition. Lower temperatures associated to this crystallisation suggested the presence of shorter chains as longer times of swelling were reached. In summary, during the water absorption process the potential crystallinity of each sample was reached, according to other studies [46].

Finally, melting enthalpy (ΔH_m) and its peak temperature (T_m) was evaluated. The tendency of this enthalpy was to slightly increase along the absorption process for all materials and temperatures, but not much than 15%. For one temperature, high filled composites showed lower enthalpy values. Melting peak temperature (T_m) did not change substantially along the water absorption procedure for any temperature, which means that always, the melting process is similar and for an equivalent crystalline nature.

From these results, it was calculated the degree of crystallinity (X_c). Thus we have a parameter to compare material structures during the whole water absorption process. The degree of crystallinity of the PLA and its composites was calculated from the first heating scan by the Equation 3.1.

$$X_c = \frac{1}{(1-m_f)} \frac{(\Delta H_m - \sum \Delta H_{cc})}{\Delta H_{m0}} \cdot 100 \qquad (3.1)$$

Where ΔH_m and ΔH_{m0} are the melting enthalpies for PLA composites and the 100% crystalline PLA, respectively; (1 - m_f) is the weight fraction of PLA in the composite and $\sum \Delta H_{cc}$ is the

summation of enthalpy of all crystallisation events. The melting enthalpy of a totally crystalline PLA material (ΔH_{m0}) was considered to be 93 J/g [50].

As suggested by Fischer et al. [31], the degree of crystallinity (X_c) increased along the water absorption process for all materials and temperatures, meaning that composite structure changed during the treatment. The increment of crystallinity degree was indicative of formation of crystalline domains. The effect of interactions with water and temperature are likely to have enhanced the mobility of the PLA chains and acted as a driving force to form crystalline structures [46]. Therefore, temperature should influenced this crystallisation process.

The reaching of the "saturation amount of crystals" (X_{cs}) was experienced faster for composites with high fiber content than for virgin PLA, as it is shown in Figures 3.16, 3.17 and 3.18. It could be due to the incorporation of fiber and its ability to act as nucleating agent, as previously commented. The influence of temperature on crystallinity degree is visible too in Figures 3.16, 3.17 and 3.18, in which for 85ºC, materials reach this "saturation amount of crystals" faster than for 75 and 65 ºC [53].

In addition, the initial proportion of crystalline phase at non degraded samples was bigger for composites than for virgin PLA, suggesting that sisal fibers acted as nucleating agent in composites during processing materials. Thus, the increment on crystallinity during the water absorption process was bigger for virgin PLA than for composites.

Table 3.10. First heating scan Saturation Crystallinity Degree (X_{cs}) for PLA and composites for different hydrothermal condition.

X_{cs} (%)	**Hydrothermal condition (ºC)**					
	65		**75**		**85**	
Fiber content (%f)	**Coupling agent**					
	Yes	**No**	**Yes**	**No**	**Yes**	**No**
0	42,0 (±1,8)		41,4 (±1,3)		38,5 (±0,1)	
10	44,6 (±3,6)	43,3 (±0,0)	45,0 (±2,6)	44,2 (±0,8)	46,6 (±1,0)	41,7 (±3,1)
20	44,3 (±0,6)	42,0 (±1,2)	45,4 (±0,9)	46,6 (±2,3)	43,4 (±1,6)	44,0 (±1,2)
30	43,3 (±0,6)	47,6 (±1,5)	44,9 (±2,6)	45,9 (±0,7)	48,6 (±0,9)	55,1 (±1,9)

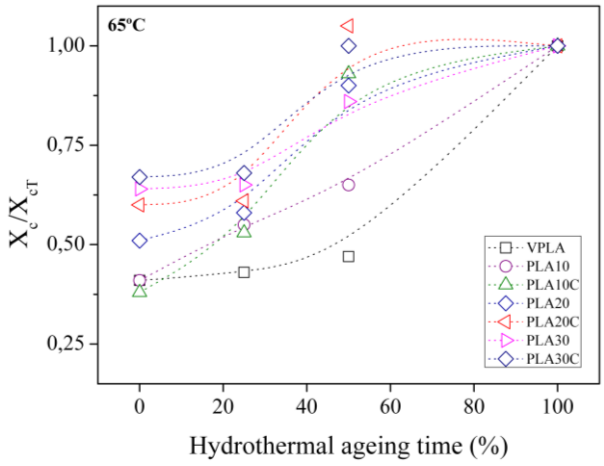

Figure 3.16. Plots of X_c/X_{cs} against % saturation for PLA and composites for 65 ºC hydrothermal condition.

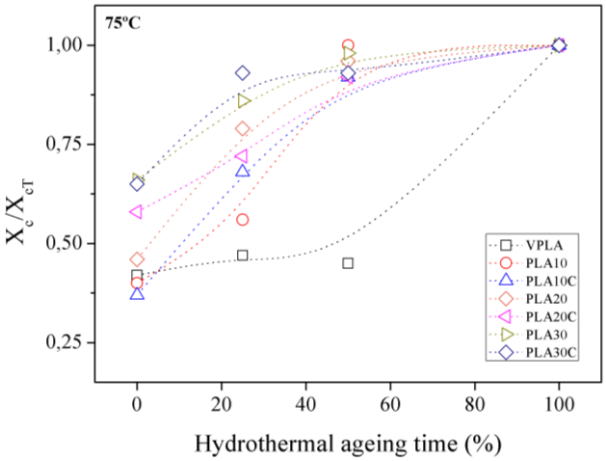

Figure 3.17. Plots of X_c/X_{cs} against % saturation for PLA and composites for 75 ºC hydrothermal condition.

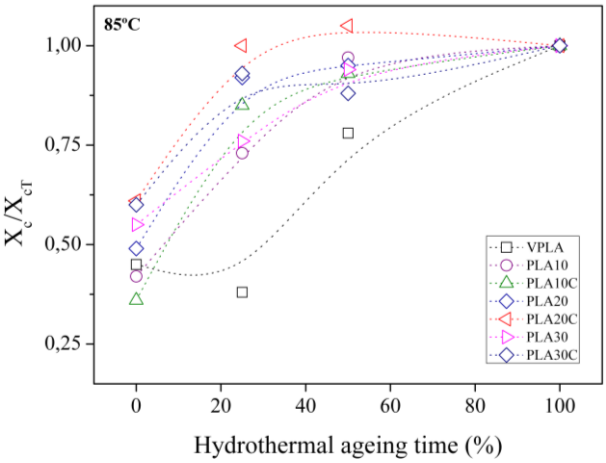

Figure 3.18. Plots of X_c/X_{cs} against % saturation for PLA and composites for 85 ºC hydrothermal condition.

From Table 3.10 it can be appreciated that composites reached bigger values of saturation crystallinity (X_{cs}), than virgin PLA. When higher was temperature, for composites with high amount of fiber, crystallinity grew. It could be related to the nucleating ability of sisal fiber in composites, as commented before, promoting the formation of more crystalline phase. However, for virgin PLA, X_{cs} reach lower values for elevated temperatures.

All this results are in concordance and corroborated suggestions on previous sections about diffusion coefficient *D*, which decreased when amount of fiber was higher for all temperatures. More crystal phase formation was favoured by sisal fiber which acted as a nucleant agent, hindering the advance of penetrant and decreasing the transport paths of the water molecules and water-interaction within the composite.

Once thermal history and water effect has been evaluated on first heating scan, cooling segment and second heating ramp will be assessed in order to analyse structure after elimination of water from the composite.

PLA based composite dynamic crystallisation and glass transition can be found on the cooling scan. Furthermore, on second heating scan, a relaxation followed by polymer cold crystallization and polymer melting can be observed on thermograms for all samples.

Process monitoring thermograms of the cooling and second heating scan in Figure 3.19 and 3.20 and calorimetric data can be found in Table 3.11, 3.12 and 3.13.

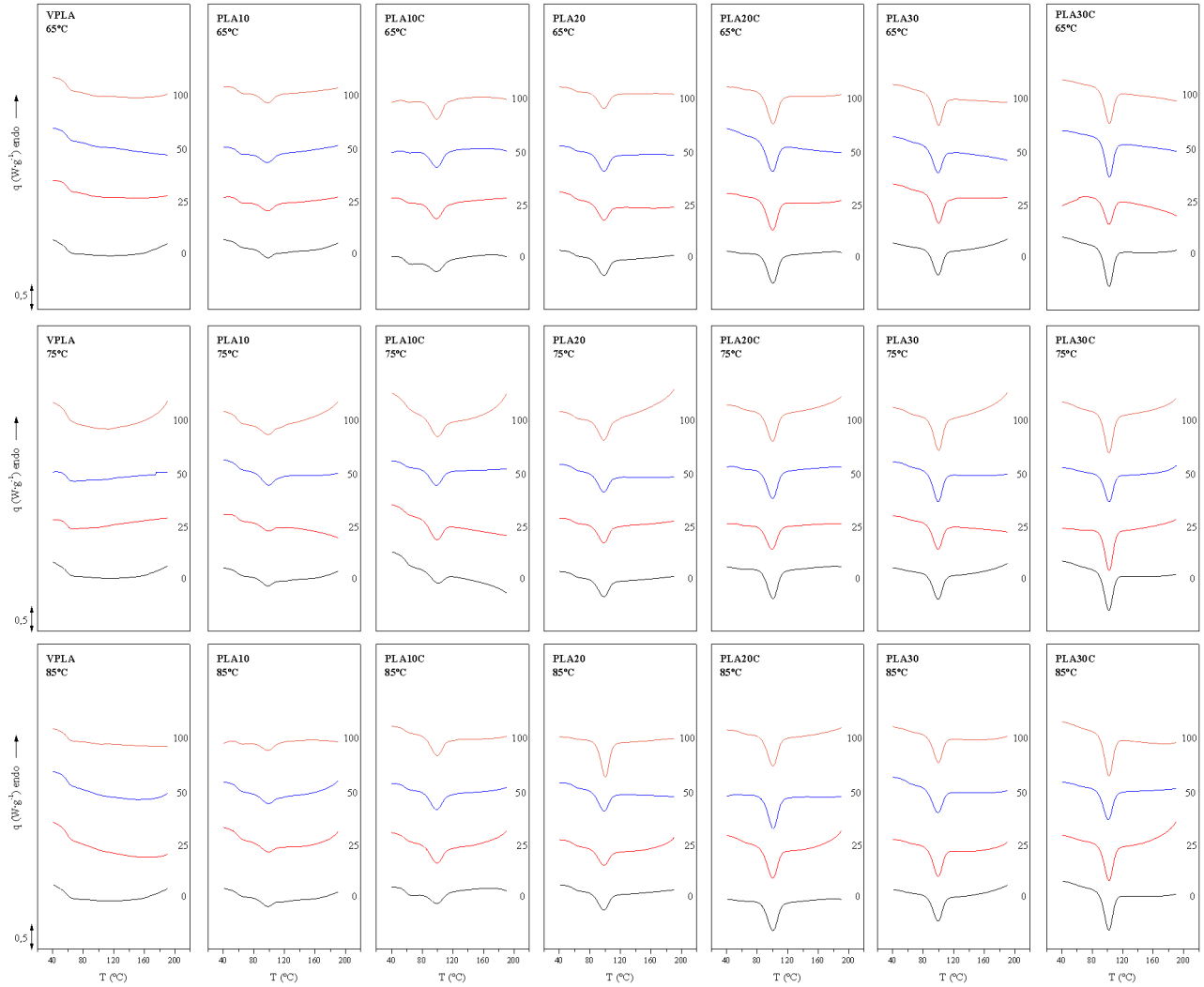

Figure 3.19. Cooling scan for PLA and composites for different hydrothermal condition (65, 75 and 85 ºC) and saturation degrees (0, 25, 50 and 100%).

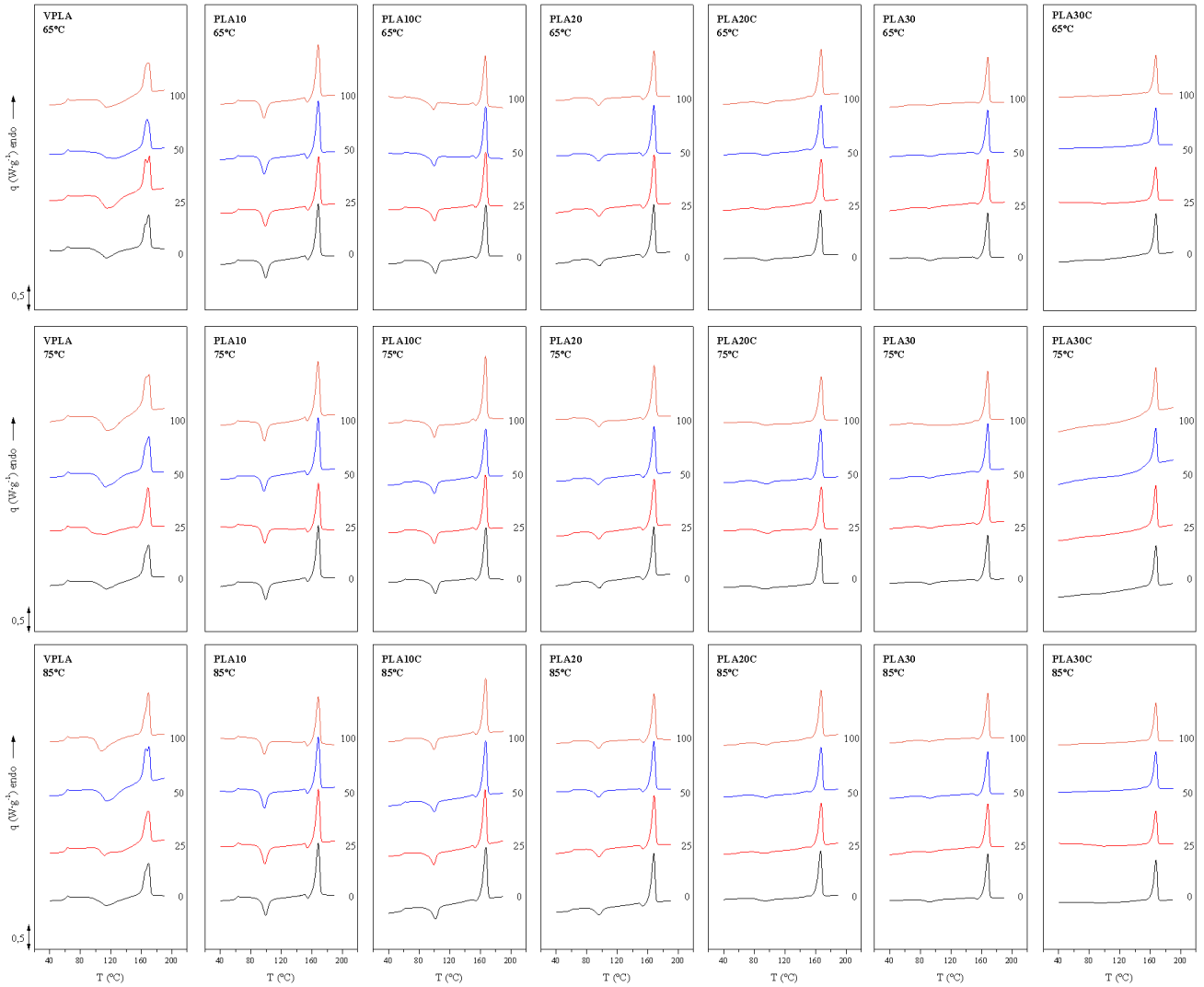

Figure 3.20. Second heating scan for PLA and composites for different hydrothermal condition (65, 75 and 85 ºC) and saturation degrees (0, 25, 50 and 100%).

Table 3.11. Cooling and second heating scan data for PLA and composites at 65 ºC and different saturation degrees.

65 ºC	Sat (%)	ΔH_{gt} (J/g)	$T_{g\text{-}p}$ (ºC)	Δc_p (J/(g·K))	T_g (ºC)	ΔH_c (J/g)	Tc (ºC)	ΔH_{cc1} (J/g)	T_{cc1} (ºC)	ΔH_{cc2} (J/g)	T_{cc2} (ºC)	ΔH_m (J/g)	T_m (ºC)	X_c (%)
VPLA	**0**	1,2 (±0,2)	63,3 (±0,1)	-0,4 (±0,1)	57,9 (±0,2)	- -	- -	-13,9 (±1,4)	113,6 (±0,1)	- -	- -	30,5 (±0,1)	169,5 (±0,2)	16,6 (±1,6)
	25	2,0 (±0,1)	63,7 (±0,1)	-0,4 (±0,1)	57,7 (±0,1)	- -	- -	-30,4 (±3,9)	114,9 (±0,3)	- -	- -	35,2 (±1,5)	169,1 (±1,4)	*4,8* *(±5,9)*
	50	1,9 (±0,1)	63,5 (±0,1)	-0,5 (±0,1)	58,1 (±0,1)	- -	- -	-32,2 (±7,7)	115,4 (±0,2)	- -	- -	34,1 (±3,2)	167,0 (±0,5)	*1,8* *(±11,7)*
	100	0,8 (±0,0)	63,5 (±0,1)	-0,4 (±0,1)	58,5 (±0,1)	- -	- -	-22,1 (±0,1)	113,2 (±1,3)	- -	- -	33,9 (±3,0)	169,5 (±0,3)	11,8 (±3,4)
PLA10	**0**	0,4 (±0,2)	62,8 (±0,1)	-0,2 (±0,1)	57,5 (±0,1)	-3,8 (±0,5)	98,1 (±0,3)	-14,7 (±2,0)	99,1 (±0,4)	-1,7 (±0,1)	154,3 (±0,1)	34,0 (±2,2)	168,1 (±0,1)	17,7 (±5,1)
	25	1,2 (±0,1)	63,5 (±0,1)	-0,3 (±0,1)	55,8 (±0,1)	-4,8 (±0,2)	97,9 (±0,2)	-16,0 (±0,3)	98,9 (±0,2)	-2,3 (±0,1)	154,5 (±0,1)	36,0 (±0,6)	168,6 (±0,1)	17,7 (±1,2)
	50	0,7 (±0,1)	63,3 (±0,1)	-0,3 (±0,1)	59,1 (±0,1)	-6,8 (±0,1)	98,1 (±0,2)	-14,5 (±0,1)	97,8 (±0,2)	-2,2 (±0,1)	153,9 (±0,2)	36,9 (±0,8)	168,4 (±0,2)	20,2 (±1,0)
	100	0,8 (±0,1)	63,2 (±0,1)	-0,3 (±0,1)	57,9 (±0,1)	-6,5 (±0,1)	98,0 (±0,1)	-15,5 (±0,1)	97,5 (±0,2)	-2,2 (±0,1)	153,9 (±0,1)	37,4 (±0,3)	168,3 (±0,1)	19,7 (±0,6)
PLA10C	**0**	0,3 (±0,1)	61,7 (±0,1)	-0,2 (±0,1)	57,3 (±0,4)	-6,8 (±0,2)	98,6 (±0,2)	-13,9 (±0,3)	101,2 (±0,3)	-0,7 (±0,1)	154,3 (±0,1)	35,9 (±0,4)	167,0 (±0,2)	21,2 (±1,0)
	25	0,7 (±0,1)	61,9 (±0,1)	-0,3 (±0,1)	54,3 (±1,2)	-10,9 (±1,6)	98,6 (±0,1)	-13,3 (±0,3)	100,5 (±0,2)	-0,8 (±0,1)	154,1 (±0,1)	36,3 (±1,8)	167,1 (±0,2)	22,2 (±2,7)
	50	0,6 (±0,1)	61,5 (±0,2)	-0,2 (±0,1)	56,2 (±0,3)	-11,9 (±0,2)	99,0 (±0,1)	-20,0 (±0,7)	99,6 (±0,1)	-0,7 (±0,1)	154,0 (±0,2)	32,0 (±2,2)	166,8 (±0,1)	11,4 (±3,6)
	100	0,3 (±0,1)	61,4 (±0,1)	-0,2 (±0,1)	56,6 (±0,2)	-15,9 (±1,8)	99,3 (±0,1)	-9,4 (±0,9)	98,7 (±0,1)	-0,8 (±0,1)	153,9 (±0,1)	35,9 (±2,5)	166,4 (±0,1)	25,8 (±4,1)
PLA20	**0**	0,2 (±0,1)	62,6 (±0,2)	- -	- -	-8,5 (±0,1)	97,9 (±0,2)	-9,3 (±0,2)	96,6 (±0,1)	-1,6 (±0,1)	153,6 (±0,2)	33,2 (±0,6)	168,0 (±0,2)	22,3 (±1,1)
	25	0,5 (±0,1)	63,1 (±0,2)	-0,2 (±0,1)	57,3 (±0,3)	-11,5 (±0,9)	98,2 (±0,0)	-9,0 (±1,0)	95,9 (±0,3)	-2,2 (±0,1)	154,0 (±0,1)	31,8 (±1,1)	168,2 (±0,1)	20,6 (±2,9)
	50	0,4 (±0,1)	62,7 (±0,1)	-0,2 (±0,1)	57,2 (±0,2)	-12,2 (±0,4)	98,8 (±0,3)	-7,4 (±0,4)	95,7 (±0,1)	-2,1 (±0,1)	153,9 (±0,1)	31,8 (±0,4)	168,0 (±0,1)	22,3 (±1,3)
	100	0,6 (±0,1)	63,0 (±0,0)	-0,2 (±0,1)	57,5 (±0,5)	-10,3 (±1,3)	98,4 (±0,1)	-7,5 (±0,6)	95,4 (±0,3)	-1,7 (±0,1)	153,6 (±0,0)	32,3 (±0,7)	168,2 (±0,1)	23,2 (±1,8)
PLA20C	**0**	- -	- -	- -	- -	-14,7 (±0,2)	100,5 (±0,1)	-3,8 (±0,3)	94,0 (±0,1)	- -	- -	30,7 (±0,6)	166,6 (±0,1)	26,9 (±1,2)
	25	0,2 (±0,1)	61,2 (±0,1)	- -	- -	-19,7 (±0,1)	100,2 (±0,1)	-2,9 (±0,3)	94,8 (±0,8)	- -	- -	31,1 (±0,1)	167,2 (±0,1)	28,2 (±0,5)
	50	- -	- -	- -	- -	-21,1 (±0,9)	100,2 (±0,3)	-2,9 (±0,5)	94,7 (±0,9)	- -	- -	32,5 (±0,7)	166,8 (±0,2)	29,6 (±1,6)
	100	0,4 (±0,1)	62,0 (±0,1)	- -	- -	-21,1 (±0,5)	100,6 (±0,2)	-3,6 (±0,0)	96,2 (±0,2)	- -	- -	32,7 (±0,1)	167,2 (±0,1)	29,1 (±0,2)
PLA30	**0**	- -	- -	- -	- -	-10,3 (±1,1)	98,9 (±0,2)	-3,4 (±0,2)	93,5 (±0,6)	-1,0 (±0,1)	154,4 (±0,1)	25,6 (±1,1)	168,2 (±0,1)	21,2 (±2,0)
	25	0,2 (±0,1)	62,3 (±0,1)	- -	- -	-17,8 (±0,3)	100,1 (±0,2)	-1,8 (±0,1)	92,5 (±0,1)	-0,9 (±0,1)	154,9 (±0,1)	28,2 (±0,2)	168,2 (±0,1)	25,5 (±0,5)
	50	0,2 (±0,1)	62,2 (±0,2)	- -	- -	-15,7 (±0,8)	99,8 (±0,4)	-2,3 (±0,5)	92,4 (±0,6)	-0,8 (±0,2)	154,5 (±0,2)	27,8 (±0,3)	168,1 (±0,1)	24,8 (±1,5)
	100	- -	- -	- -	- -	-17,3 (±0,1)	100,0 (±0,1)	-2,1 (±0,3)	92,6 (±0,1)	-0,6 (±0,1)	154,8 (±0,2)	29,5 (±0,7)	168,1 (±0,2)	26,8 (±1,7)
PLA30C	**0**	- -	- -	- -	- -	-18,5 (±0,1)	101,8 (±0,1)	- -	- -	- -	- -	26,9 (±0,4)	167,4 (±0,0)	26,9 (±0,6)
	25	- -	- -	- -	- -	-16,8 (±2,9)	101,9 (±0,2)	- -	- -	- -	- -	26,0 (±1,8)	167,4 (±0,2)	26,0 (±2,8)
	50	- -	- -	- -	- -	-21,1 (±0,9)	100,2 (±0,3)	- -	- -	- -	- -	27,5 (±0,2)	167,2 (±0,1)	27,5 (±0,4)
	100	0,4 (±0,1)	62,0 (±0,1)	- -	- -	-21,1 (±0,5)	100,6 (±0,2)	- -	- -	- -	- -	28,2 (±1,0)	167,5 (±0,1)	28,2 (±1,5)

Table 3.12. Cooling and second heating scan data for PLA and composites at 75 ºC and different saturation degrees.

75 ºC	Sat (%)	ΔH_{gt} (J/g)	$T_{g\text{-}p}$ (ºC)	Δc_p (J/(g·K))	T_g (ºC)	ΔH_c (J/g)	Tc (ºC)	ΔH_{cc1} (J/g)	T_{cc1} (ºC)	ΔH_{cc2} (J/g)	T_{cc2} (ºC)	ΔH_m (J/g)	T_m (ºC)	X_c (%)
VPLA	**0**	1,2 (±0,2)	63,3 (±0,1)	-0,4 (±0,1)	57,9 (±0,2)	- -	- -	-13,9 (±1,4)	113,6 (±0,1)	- -	- -	30,5 (±0,1)	169,5 (±0,2)	16,6 (±1,6)
	25	1,3 (±0,1)	63,3 (±0,1)	-0,4 (±0,1)	58,1 (±0,1)	- -	- -	-19,2 (±2,3)	112,7 (±0,7)	-0,5 (±0,1)	153,5 (±0,1)	30,3 (±3,4)	168,6 (±0,2)	10,6 (±6,0)
	50	1,0 (±0,1)	63,4 (±0,1)	-0,4 (±0,1)	58,2 (±0,1)	- -	- -	-22,2 (±8,0)	113,2 (±0,1)	- -	- -	32,5 (±5,1)	169,6 (±0,2)	10,3 (±14,0)
	100	1,0 (±0,1)	63,4 (±0,1)	-0,5 (±0,1)	58,0 (±0,1)	- -	- -	-27,5 (±2,8)	114,2 (±0,5)	- -	- -	38,0 (±3,0)	169,0 (±0,8)	10,5 (±6,1)
PLA10	**0**	0,4 (±0,2)	62,8 (±0,1)	-0,2 (±0,0)	57,5 (±0,1)	-3,8 (±0,5)	98,1 (±0,3)	-14,7 (±2,0)	99,1 (±0,4)	-1,7 (±0,1)	154,3 (±0,1)	34,0 (±2,2)	168,1 (±0,1)	17,7 (±5,1)
	25	0,7 (±0,1)	63,1 (±0,1)	-0,3 (±0,1)	57,1 (±0,2)	-4,0 (±0,4)	98,3 (±0,1)	-15,9 (±1,0)	98,3 (±0,2)	-2,1 (±0,1)	154,1 (±0,1)	35,4 (±2,3)	168,3 (±0,1)	17,4 (±4,0)
	50	0,4 (±0,1)	62,8 (±0,1)	-0,3 (±0,1)	57,3 (±0,1)	-8,7 (±0,2)	98,8 (±0,3)	-14,3 (±0,1)	97,4 (±0,1)	-1,9 (±0,1)	153,9 (±0,1)	38,3 (±0,2)	168,1 (±0,1)	22,0 (±0,3)
	100	0,6 (±0,1)	62,9 (±0,2)	-0,4 (±0,1)	57,3 (±0,1)	-7,5 (±0,4)	98,4 (±0,1)	-17,5 (±0,1)	97,7 (±0,1)	-1,4 (±0,1)	153,7 (±0,4)	41,9 (±0,2)	168,1 (±0,4)	23,0 (±0,5)
PLA10C	**0**	0,3 (±0,1)	61,7 (±0,1)	-0,2 (±0,1)	57,3 (±0,4)	-6,8 (±0,2)	98,6 (±0,2)	-13,9 (±0,3)	101,2 (±0,3)	-0,7 (±0,1)	154,3 (±0,1)	35,9 (±0,4)	167,0 (±0,2)	21,2 (±1,0)
	25	0,8 (±0,1)	61,1 (±0,2)	-0,3 (±0,1)	54,1 (±0,5)	-13,2 (±0,5)	98,7 (±0,1)	-10,9 (±1,7)	99,5 (±0,3)	-0,5 (±0,2)	153,8 (±0,1)	36,2 (±1,9)	166,6 (±0,1)	24,9 (±4,6)
	50	0,3 (±0,1)	61,0 (±0,5)	-0,2 (±0,1)	54,3 (±0,3)	-13,8 (±1,9)	98,8 (±0,3)	-11,2 (±1,1)	99,2 (±1,0)	-0,6 (±0,1)	153,9 (±0,1)	34,9 (±0,9)	166,7 (±0,3)	23,1 (±2,4)
	100	0,6 (±0,1)	61,9 (±0,1)	-0,3 (±0,1)	56,5 (±0,7)	-16,0 (±0,2)	99,3 (±0,1)	-10,9 (±1,1)	99,9 (±0,1)	-0,4 (±0,1)	153,9 (±0,3)	40,0 (±2,7)	167,0 (±0,3)	28,8 (±4,6)
PLA20	**0**	0,2 (±0,1)	62,6 (±0,2)	- -	- -	-8,5 (±0,1)	97,9 (±0,2)	-9,3 (±0,2)	96,6 (±0,1)	-1,6 (±0,1)	153,6 (±0,2)	33,2 (±0,6)	168,0 (±0,2)	22,3 (±1,1)
	25	0,4 (±0,1)	62,7 (±0,1)	-0,2 (±0,1)	56,0 (±1,5)	-10,4 (±0,4)	98,1 (±0,1)	-7,6 (±0,4)	96,0 (±0,1)	-1,1 (±0,1)	154,0 (±0,1)	32,4 (±1,8)	168,2 (±0,2)	23,7 (±3,2)
	50	0,4 (±0,1)	63,0 (±0,1)	-0,2 (±0,1)	55,4 (±0,9)	-11,3 (±0,9)	98,0 (±0,1)	-9,7 (±1,1)	95,5 (±0,3)	-1,7 (±0,1)	153,4 (±0,1)	34,0 (±0,8)	168,1 (±0,1)	22,6 (±2,7)
	100	0,2 (±0,1)	62,4 (±0,3)	-0,2 (±0,1)	55,9 (±0,6)	-15,9 (±0,6)	98,7 (±0,4)	-5,4 (±1,1)	95,8 (±0,1)	-0,9 (±0,1)	153,8 (±0,2)	35,8 (±2,3)	168,1 (±0,1)	29,6 (±4,8)
PLA20C	**0**	- -	- -	- -	- -	-14,7 (±0,2)	100,5 (±0,1)	-3,8 (±0,3)	94,0 (±0,1)	- -	- -	30,7 (±0,6)	166,6 (±0,1)	26,9 (±1,2)
	25	0,4 (±0,1)	61,8 (±0,1)	-0,2 (±0,1)	51,3 (±0,8)	-19,2 (±1,6)	99,8 (±0,2)	-4,2 (±0,7)	96,6 (±0,8)	-0,6 (±0,1)	153,2 (±0,1)	31,6 (±0,2)	167,3 (±0,1)	26,8 (±1,3)
	50	0,2 (±0,1)	61,6 (±0,2)	-0,1 (±0,1)	56,4 (±0,3)	-19,3 (±0,0)	100,3 (±0,1)	-3,4 (±0,6)	95,6 (±0,8)	-0,4 (±0,1)	153,3 (±0,2)	32,7 (±1,1)	167,1 (±0,2)	28,9 (±2,6)
	100	0,4 (±0,1)	62,3 (±0,2)	- -	- -	-12,7 (±0,3)	98,6 (±0,3)	-6,6 (±0,1)	95,2 (±0,3)	-1,2 (±0,2)	153,6 (±0,1)	33,6 (±0,3)	167,8 (±0,1)	25,8 (±0,7)
PLA30	**0**	- -	- -	- -	- -	-10,3 (±1,1)	98,9 (±0,2)	-3,4 (±0,2)	93,5 (±0,6)	-1,0 (±0,1)	154,4 (±0,1)	25,6 (±1,1)	168,2 (±0,1)	21,2 (±2,0)
	25	0,0 (±0,1)	62,0 (±0,2)	- -	- -	-16,3 (±1,4)	99,3 (±0,1)	-3,4 (±0,2)	93,2 (±0,3)	-1,1 (±0,1)	154,4 (±0,1)	29,7 (±1,9)	167,8 (±0,1)	25,1 (±3,4)
	50	- -	- -	- -	- -	-17,2 (±0,6)	99,3 (±0,2)	-3,0 (±0,1)	92,8 (±0,5)	-0,7 (±0,1)	153,9 (±0,7)	30,7 (±0,7)	168,0 (±0,2)	27,1 (±1,4)
	100	- -	- -	- -	- -	-20,1 (±0,5)	100,1 (±0,1)	-0,7 (±0,1)	92,3 (±0,4)	-0,2 (±0,1)	154,3 (±0,2)	31,9 (±0,7)	167,7 (±0,1)	31,0 (±1,2)
PLA30C	**0**	- -	- -	- -	- -	-18,5 (±0,1)	101,8 (±0,1)	- -	- -	- -	- -	26,9 (±0,4)	167,4 (±0,1)	26,9 (±0,6)
	25	- -	- -	- -	- -	-20,9 (±0,5)	101,8 (±0,6)	- -	- -	- -	- -	30,0 (±0,3)	167,2 (±0,2)	30,0 (±0,5)
	50	- -	- -	- -	- -	-19,7 (±0,7)	102,2 (±0,4)	- -	- -	- -	- -	29,1 (±0,5)	167,0 (±0,2)	29,1 (±0,7)
	100	- -	- -	- -	- -	-22,0 (±1,2)	102,3 (±0,2)	- -	- -	- -	- -	31,1 (±2,6)	167,1 (±0,1)	31,1 (±4,1)

Table 3.13. Cooling and second heating scan data for PLA and composites at 85 ºC and different saturation degrees.

85 ºC	Sat (%)	ΔH_{gt} (J/g)	$T_{g\text{-}p}$ (ºC)	Δc_p (J/(g·K))	T_g (ºC)	ΔH_c (J/g)	Tc (ºC)	ΔH_{cc1} (J/g)	T_{cc1} (ºC)	ΔH_{cc2} (J/g)	T_{cc2} (ºC)	ΔH_m (J/g)	T_m (ºC)	X_c (%)
VPLA	0	1,2 (±0,2)	63,3 (±0,1)	-0,4 (±0,1)	57,9 (±0,2)	- -	- -	-13,9 (±1,4)	113,6 (±0,1)	- -	- -	30,5 (±0,1)	169,5 (±0,2)	16,6 (±1,6)
	25	1,1 (±0,1)	63,2 (±0,1)	-0,5 (±0,1)	57,5 (±0,3)	- -	- -	-18,7 (±3,4)	110,1 (±1,5)	- -	- -	32,1 (±0,3)	168,9 (±0,5)	13,4 (±4,0)
	50	0,7 (±0,1)	63,2 (±0,1)	-0,4 (±0,1)	57,7 (±0,1)	- -	- -	-26,2 (±3,6)	112,7 (±1,6)	- -	- -	39,1 (±0,9)	169,5 (±0,5)	12,9 (±4,8)
	100	- -	- -	-0,4 (±0,1)	57,8 (±0,3)	- -	- -	-27,8 (±1,9)	109,8 (±2,0)	- -	- -	36,3 (±0,4)	169,1 (±0,1)	8,4 (±2,4)
PLA10	0	0,4 (±0,2)	62,8 (±0,1)	-0,2 (±0,1)	57,5 (±0,1)	-3,8 (±0,5)	98,1 (±0,3)	-14,7 (±2,0)	99,1 (±0,4)	-1,7 (±0,1)	154,3 (±0,1)	34,0 (±2,2)	168,1 (±0,1)	17,7 (±5,1)
	25	0,7 (±0,1)	63,2 (±0,1)	-0,4 (±0,1)	57,6 (±0,1)	-5,7 (±0,0)	98,3 (±0,2)	-18,0 (±0,2)	98,5 (±0,3)	-2,4 (±0,1)	154,3 (±0,3)	36,6 (±0,1)	168,5 (±0,2)	16,2 (±0,5)
	50	0,8 (±0,1)	62,9 (±0,1)	-0,3 (±0,1)	57,3 (±0,1)	-4,4 (±0,2)	98,3 (±0,0)	-15,4 (±0,5)	97,7 (±0,1)	-1,9 (±0,1)	154,0 (±0,1)	36,6 (±0,9)	168,3 (±0,2)	19,3 (±1,7)
	100	0,9 (±0,1)	63,1 (±0,1)	-0,3 (±0,1)	57,0 (±0,3)	-3,9 (±0,0)	98,4 (±0,2)	-14,2 (±1,2)	98,0 (±0,1)	-2,2 (±0,1)	154,3 (±0,1)	35,0 (±2,2)	168,4 (±0,1)	18,5 (±4,2)
PLA10C	0	0,3 (±0,1)	61,7 (±0,1)	-0,2 (±0,1)	57,3 (±0,4)	-6,8 (±0,2)	98,6 (±0,2)	-13,9 (±0,3)	101,2 (±0,3)	-0,7 (±0,1)	154,3 (±0,1)	35,9 (±0,4)	167,0 (±0,2)	21,2 (±1,0)
	25	0,2 (±0,1)	61,7 (±0,1)	-0,3 (±0,1)	54,4 (±0,3)	-9,9 (±0,8)	99,0 (±0,2)	-11,2 (±0,7)	100,0 (±0,2)	-0,9 (±0,1)	153,8 (±0,1)	36,8 (±0,7)	166,8 (±0,1)	24,7 (±1,7)
	50	0,3 (±0,1)	61,5 (±0,1)	-0,2 (±0,1)	55,8 (±1,0)	-9,5 (±0,6)	98,7 (±0,1)	-11,0 (±1,1)	99,9 (±0,1)	-0,7 (±0,1)	154,0 (±0,1)	35,6 (±3,1)	167,1 (±0,1)	23,9 (±5,3)
	100	0,5 (±0,1)	62,0 (±0,1)	-0,2 (±0,1)	58,0 (±0,1)	-10,8 (±0,3)	99,2 (±0,1)	-12,3 (±0,1)	99,8 (±0,2)	-1,0 (±0,1)	154,3 (±0,1)	37,0 (±0,4)	166,9 (±0,1)	23,7 (±0,6)
PLA20	0	0,2 (±0,1)	62,6 (±0,2)	- -	- -	-8,5 (±0,1)	97,9 (±0,2)	-9,3 (±0,2)	96,6 (±0,1)	-1,6 (±0,1)	153,6 (±0,2)	33,2 (±0,6)	168,0 (±0,2)	22,3 (±1,1)
	25	0,3 (±0,1)	62,6 (±0,2)	-0,2 (±0,1)	55,1 (±1,1)	-8,7 (±0,6)	98,3 (±0,1)	-8,0 (±0,1)	95,6 (±0,2)	-1,3 (±0,1)	153,2 (±0,2)	32,2 (±0,9)	167,9 (±0,1)	23,0 (±1,4)
	50	0,3 (±0,1)	62,5 (±0,1)	-0,2 (±0,1)	56,7 (±0,1)	-10,4 (±0,1)	98,5 (±0,1)	-5,9 (±0,4)	95,2 (±0,1)	-1,6 (±0,2)	153,7 (±0,3)	32,4 (±0,6)	168,0 (±0,3)	24,9 (±1,7)
	100	0,1 (±0,1)	61,7 (±0,3)	- -	- -	-16,1 (±1,3)	100,0 (±0,3)	-2,0 (±0,4)	93,7 (±0,4)	-0,6 (±0,1)	155,4 (±0,1)	27,6 (±0,4)	168,1 (±0,3)	25,0 (±1,1)
PLA20C	0	- -	- -	- -	- -	-14,7 (±0,2)	100,5 (±0,1)	-3,8 (±0,3)	94,0 (±0,1)	- -	- -	30,7 (±0,6)	166,6 (±0,1)	26,9 (±1,2)
	25	0,3 (±0,1)	61,6 (±0,2)	- -	- -	-16,0 (±1,5)	100,0 (±0,3)	-2,7 (±0,3)	96,6 (±0,7)	-0,4 (±0,0)	153,1 (±0,1)	33,4 (±0,6)	167,3 (±0,2)	30,3 (±1,3)
	50	0,2 (±0,1)	61,8 (±0,1)	- -	- -	-18,3 (±0,2)	100,5 (±0,4)	-2,8 (±0,8)	94,6 (±0,4)	-0,2 (±0,1)	153,1 (±0,4)	33,5 (±2,3)	167,0 (±0,1)	30,5 (±4,3)
	100	0,2 (±0,1)	62,0 (±0,1)	- -	- -	-16,8 (±0,5)	100,4 (±0,0)	-3,9 (±0,3)	96,7 (±0,1)	-0,5 (±0,1)	153,4 (±0,1)	33,7 (±1,2)	167,2 (±0,1)	29,3 (±2,1)
PLA30	0	- -	- -	- -	- -	-10,3 (±1,1)	98,9 (±0,2)	-3,4 (±0,2)	93,5 (±0,6)	-1,0 (±0,1)	154,4 (±0,1)	25,6 (±1,1)	168,2 (±0,1)	21,2 (±2,0)
	25	0,1 (±0,1)	61,8 (±0,3)	- -	- -	-13,7 (±1,4)	99,4 (±0,1)	-2,3 (±0,1)	92,8 (±0,1)	-0,7 (±0,1)	154,4 (±0,1)	27,3 (±2,3)	168,1 (±0,1)	24,4 (±3,6)
	50	0,2 (±0,1)	62,5 (±0,1)	- -	- -	-15,3 (±0,2)	99,1 (±0,0)	-6,3 (±0,2)	95,6 (±0,1)	-1,7 (±0,1)	153,9 (±0,1)	34,7 (±0,2)	167,8 (±0,1)	26,6 (±0,8)
	100	0,1 (±0,1)	62,1 (±0,1)	- -	- -	-14,2 (±0,3)	99,7 (±0,1)	-1,7 (±0,5)	92,6 (±0,1)	-0,9 (±0,2)	155,1 (±0,2)	25,7 (±1,4)	168,2 (±0,1)	23,1 (±3,2)
PLA30C	0	- -	- -	- -	- -	-18,5 (±0,1)	101,8 (±0,1)	- -	- -	- -	- -	26,9 (±0,4)	167,4 (±0,1)	26,9 (±0,6)
	25	0,3 (±0,1)	62,7 (±0,6)	- -	- -	-18,5 (±0,6)	102,0 (±0,3)	- -	- -	- -	- -	29,2 (±0,3)	167,1 (±0,1)	29,2 (±0,5)
	50	0,1 (±0,1)	61,7 (±0,2)	- -	- -	-16,1 (±0,1)	101,0 (±0,3)	- -	- -	- -	- -	28,2 (±2,0)	167,3 (±0,1)	28,2 (±3,2)
	100	0,1 (±0,1)	61,5 (±0,3)	- -	- -	-19,9 (±1,0)	101,5 (±0,4)	- -	- -	- -	- -	31,1 (±0,7)	167,6 (±0,1)	31,1 (±1,2)

From DSC cooling scan, the crystallisation enthalpy and temperature peak, the glass transition and specific heat capacity was obtained.

The crystallisation phenomenon occurred at higher temperatures during cooling scan when fiber content and water saturation mass increased. For composites T_c was 2-4 ºC higher than for VPLA, but the increment was about 1 ºC from 0% to 100% water saturated samples. Enthalpy for this crystallisation process (ΔH_c) was substantially bigger for composites with high amount of fiber as well as for more saturated samples. It is related to the ability of fiber to act as nucleating agents for crystallisation [39] and to the chain scissions processes occurred along the hydrothermal treatment. All this effects were influenced by temperature, which promoted interactions with water and acted as a driving force to form crystalline structures [46].

The next event during cooling is the glass transition. For composites, this episode turned to lower temperatures, even disappearing on thermograms for big amount of fiber (PLA30/30C). Specific heat capacity (Δc_P) associated to this transition decreased along the water absorption process as well as T_g did, even disappearing for high amounts of fiber (PLA30/30C).

Crystallisation and glass transition events are closely related. While first one is based on crystal phase, the second one is on amorphous phase. Thus, when higher is the amount of crystal formed during cooling scan, the less significant is the glass transition.

Therefore, these results suggested that, on the one hand, composites with high amount of fiber seem to be more degraded because of the fiber presence, which allows more water penetration. On the other hand, the nucleating ability of sisal fiber is an important phenomenon too of high fibered composites. Two both phenomena allowed materials to reach high crystalline contents during cooling scan. It is important to remark that hydrothermal condition influenced only in the rate in which parameters change. It could be defined as a kinetic effect. For high temperatures, parameters changed faster than for lower ones.

From DSC second heating scan, cold crystallisation and melting phenomena were evaluated in order to know material changes in samples before and after hydrothermal treatment, once absorbed water was removed on first heating scan. All these parameters and transitions will be very closely related to the previous heating scan during DSC experiment.

About cold crystallisation event, it appeared about 20 ºC earlier for composites with high amount of fiber (PLA30) than for VPLA. T_{cc1} decreased about 1 ºC for all materials along the

absorption process. The same tendency was observed for enthalpy associated to crystallisation progress. ΔH_{cc1} decreased as bigger is fiber content, even disappearing for PLA30C. This cold crystallisation phenomenon could not be found for this material presumably because all polymer phase available to crystallize did it during the previous cooling scan.

The next transition in thermograms was the melting of the polymeric crystal phase, which temperature peak (T_m) decreased from ~169 to ~167 ºC when fiber content was bigger. This temperature did not change substantially along the water absorption process for any material. Enthalpy associated to this transition (ΔH_m) was higher as water saturation increased, meaning a higher amount of crystal phase. The enthalpy difference between unsaturated samples and saturated ones was bigger for VPLA (from 4 to 8 J/g) than for composites (from 3 to 6 J/g). This enthalpy was lower for composites with high amount of fiber.

As done before for the first heating scan, it was calculated the crystallinity degree (X_c) for all samples and materials. X_c reached bigger values when fiber content increased. There was a wide difference between crystallinity for VPLA and PLA30/30C, being three times bigger for composite with higher amount of fiber. The reason for these results is presumably again the ability of fiber to act as nucleating agents for crystallisation [53] and to the presumably chain scissions processes occurred along the hydrothermal treatment [46]. X_c values for saturated samples in second heating scan are shown in Table 3.14.

Table 3.14. Second heating scan Saturation Crystallinity Degree (X_{cs}) for PLA and composites at various temperatures.

X_{cs} (%)	**Hydrothermal condition (ºC)**					
	65		**75**		**85**	
Fiber content (%f)	**Coupling agent**					
	Yes	**No**	**Yes**	**No**	**Yes**	**No**
0	12,7 (±3,4)		11,2 (±6,1)		9,1 (±2,5)	
10	31,4 (±4,1)	23,5 (±0,6)	35,1 (±4,6)	27,5 (±0,5)	29,0 (±0,6)	22,1 (±4,2)
20	39,1 (±0,2)	31,9 (±1,8)	34,6 (±0,7)	40,7 (±4,8)	39,3 (±2,1)	34,4 (±1,1)
30	44,6 (±1,5)	41,1 (±1,7)	49,1 (±4,1)	47,5 (±1,2)	49,1 (±1,2)	35,5 (±3,2)

3.4 Superficial morphology

In order to obtain visual consequences caused by hydrodegradation process for all temperatures, the same samples used in DSC analysis were monitored by scanning electron microscopy (SEM). Micrographs gave a visual explanation about increment showed on water saturation mass M_s for composites for all hydrothermal conditions as well as the increment in permeability coefficient showed in previous sections.

Figure 3.21, 3.22 and 3.23 display the surface morphologies of VPLA and composites after hydrothermal ageing at different temperatures. After immersion, a smoother surface than at the beginning was observed, due to the temperature above T_g, at which polymer chains become reorganized and relaxed.

In general terms, superficial morphology analysis showed an important physical degradation promoted by absorbed water, effect of sisal fiber and temperature during hydrothermal treatment. Free water decreased and bound water increased as water is absorbed excessively [37]. This is the case of the PLA/sisal biocomposites, for all compositions and temperatures.

For composites with natural fibers, degradation process occurred when swelling of cellulose fibers developed stress at interface regions leading to microcracking mechanism in the matrix around swollen fibers and this promoted capillarity and transport via microcracks [38], as suggested in previous sections. The cracking effect was higher for high amount of fiber and temperature, as it can be seen in micrographs. When temperature was higher in water environment, microcracks on the surface and in the bulk of the material developed leading to peeling and surface dissolution of the composite [38].

Coupling agent promoted slightly smaller cracks on materials where it was incorporated.

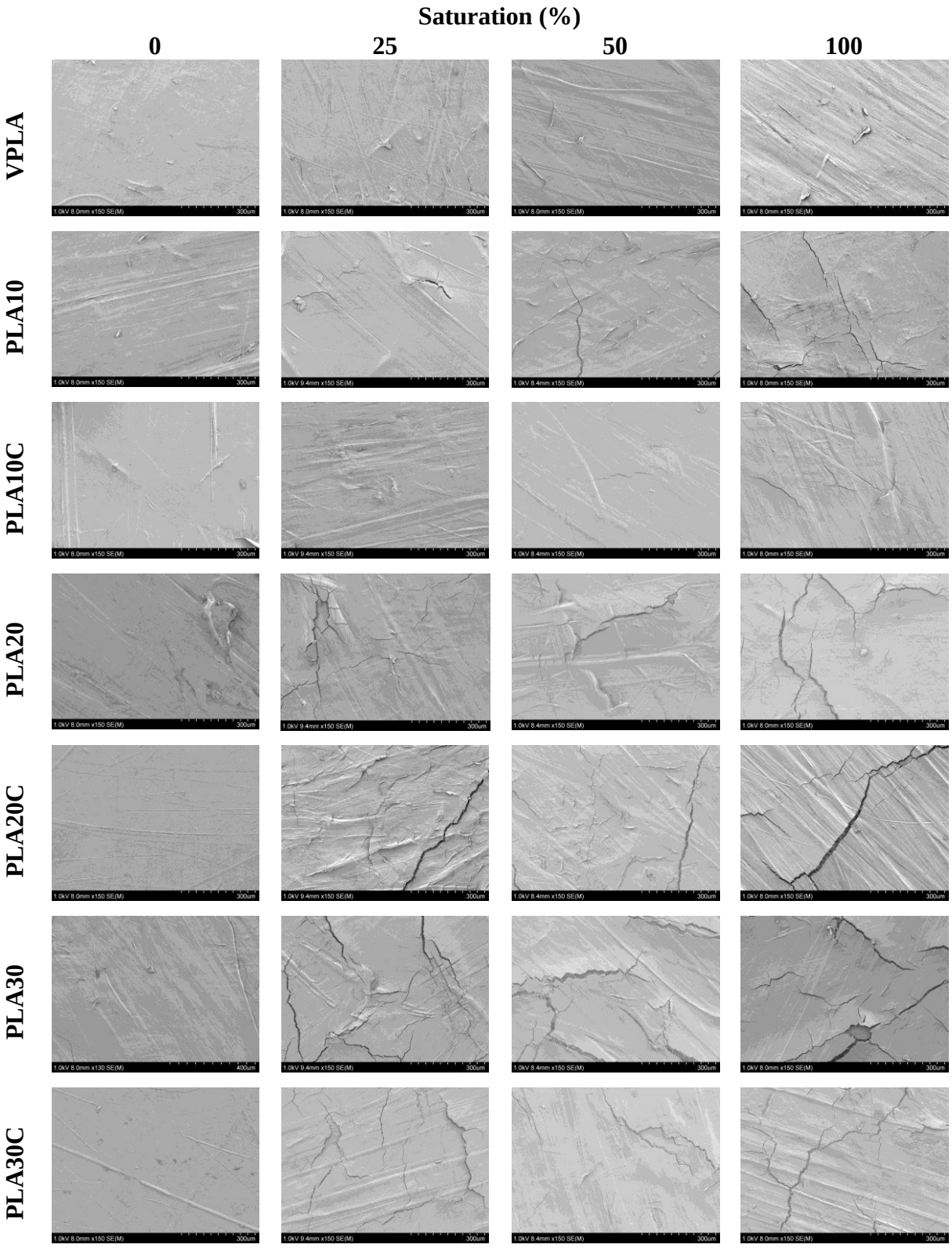

Figure 3.21. Micrographs for VPLA and composites at 65 ºC for different saturation degrees.

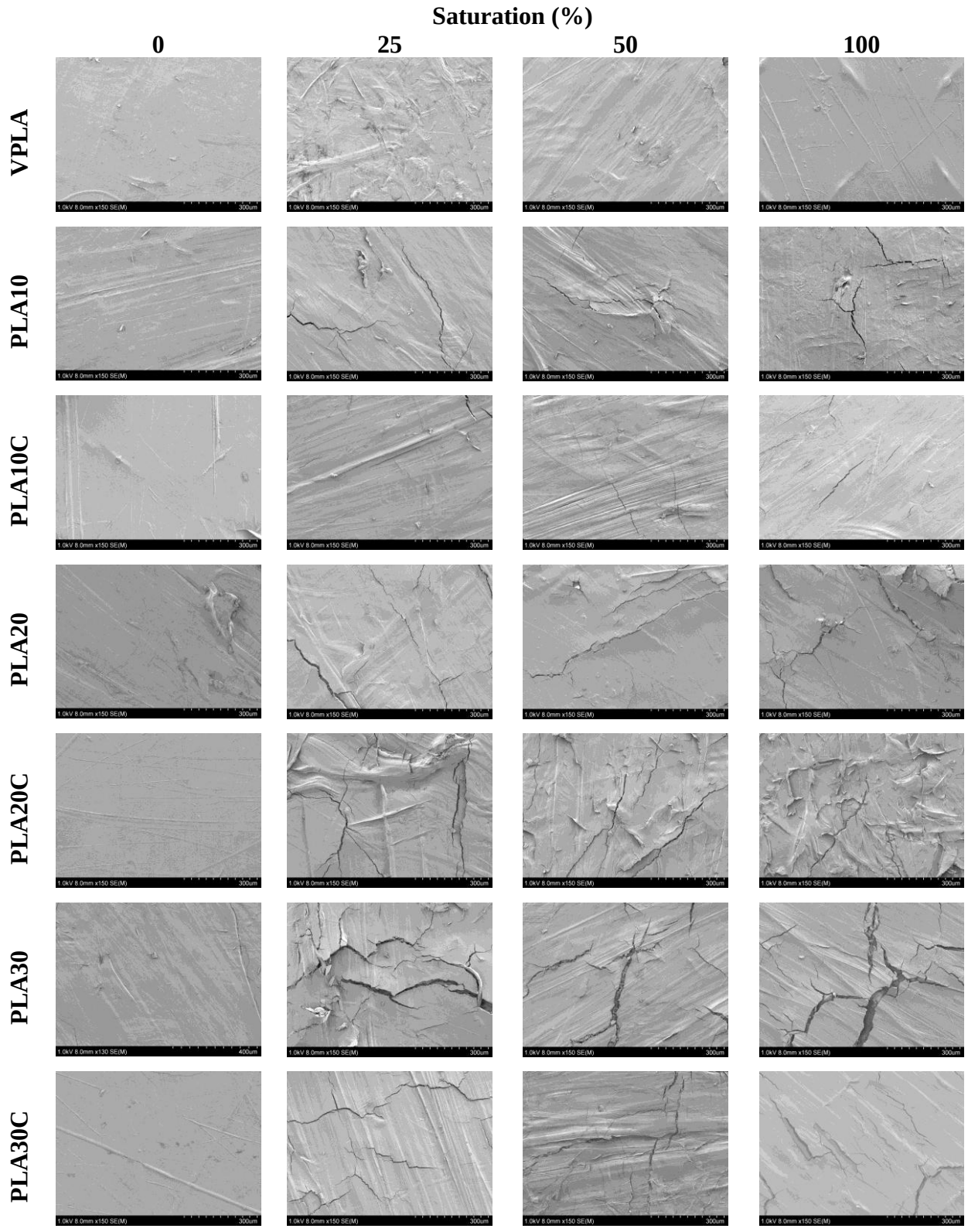

Figure 3.22. Micrographs for VPLA and composites at 75 ºC for different saturation degrees.

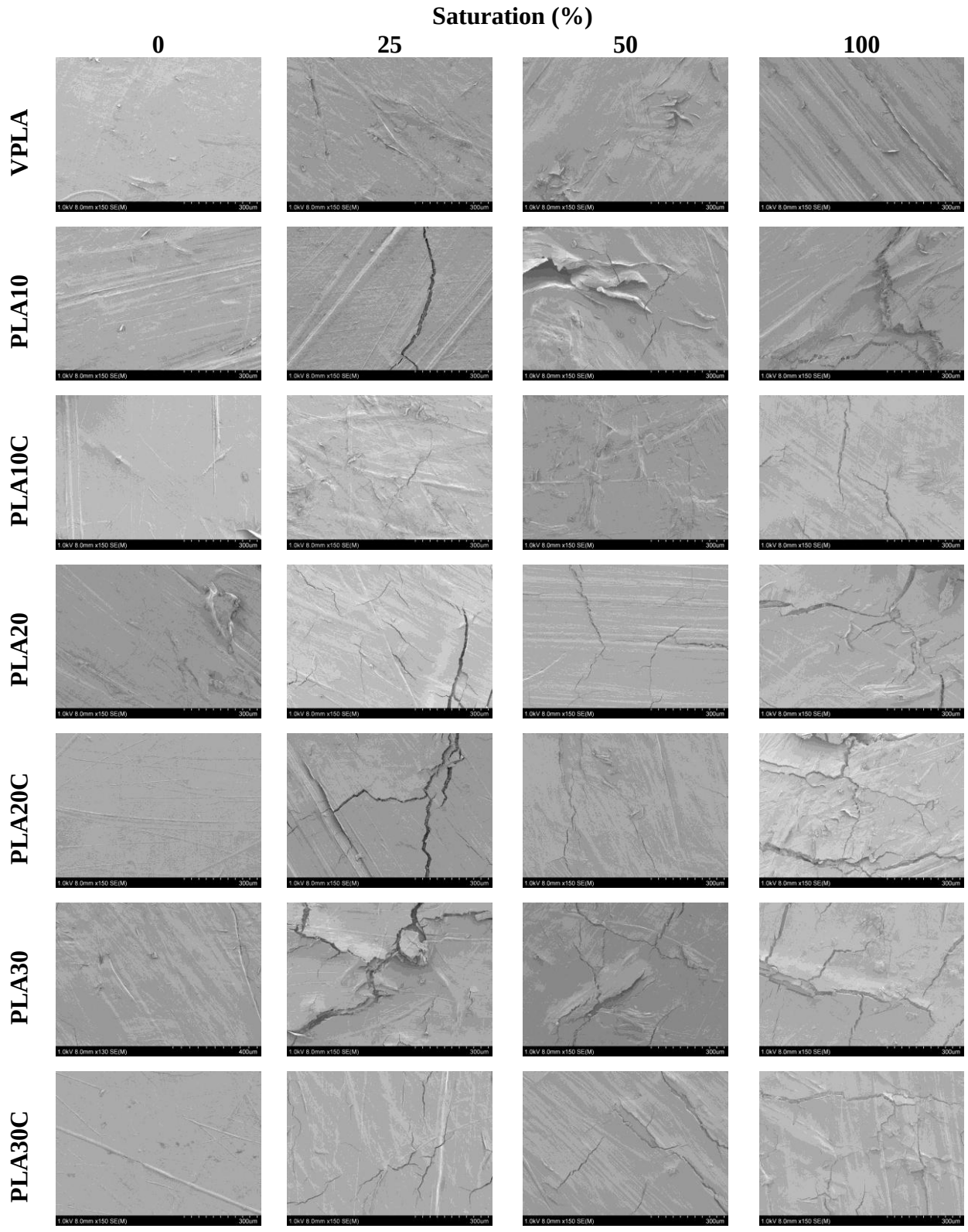

Figure 3.23. Micrographs for VPLA and composites at 85 ºC for different saturation degrees.

4. Conclusions

The application of normalized water absorption experiments was useful to simulate and monitor the degradation induced by accelerated hydrothermal treatment on PLA/sisal biocomposites at temperatures above the glass transition. In general terms, an important physical degradation promoted by absorbed water, temperature and effect of sisal fiber was produced by the hydrothermal treatment.

Concerning water absorption behaviour, on the one hand it was found that sisal fiber composites reached bigger percentage of saturation mass for all thermal conditions. On the other hand, as expected, the diffusion coefficient increased with the temperature of the hydrothermal condition. However, it decreased in composites due to the formation of crystalline domains in PLA matrix, caused by sisal fiber, which acted as a nucleating agent. In addition, Differential Scanning Calorimetry analysis showed that the presence of water into the polymer matrices displaced the glass transition towards lower temperatures due to plasticization of the polymeric phase.

The Thermo-Gravimetric analysis showed non-significant chemical changes neither in the PLA matrix back-bone nor in sisal fiber.

Surface analysis by Scanning Electron Microscopy showed an important physical degradation promoted by the formation of cracks around swollen fibers. It promoted capillarity and transport via microcracks resulting in a high amount of water absorbed percentage. This effect was more relevant the higher the fiber content was.

Maleic anhydride used as a coupling agent slightly promoted smaller cracks on the PLA/sisal biocomposites. Technologically speaking, the use of maleic anhydride did not improve the biocomposite performance. There is an important investigation field in this direction to improve the compatibility between PLA and natural fibers as sisal.

References

[1] Drumright R. E., Patrick R. G., and David H. "Polylactic Acid Technology" Advanced Materials, 2000, 12(23):1841-1846.

[2] Mapleston P., "Environmentally degrading: Bioplastics in Europe" (part 2). Plastics Engineering Europe Spring, pag. 24-29, 2006.

[3] Mapleston P., "Following the green line: Bioplastics in Europe". Plastics Engineering Europe Winter, pag. 14-19, 2005.

[4] Gu S., Yang M., Yu T., Ren T., Ren J. *Synthesis and characterization of biodegradable lactic acid-based polymers by chain extension*. J Polym Int, 2008, 57: 982-986.

[5] Tadashi Y., Masayuki Y. *Structure and properties for biomass-based polyester blends of PLA and PBS*. Eur Polym J, 2008, 44: 677-685.

[6] Masud S. H., Lawrence T. D., Manjusri M. *A study on biocomposites from recycled newspaper fiber and poly(lactic acid)*. Ind Eng Chem Res, 2005, 44: 5593-5601.

[7] Smita M., Sushil K. V., Sanjay K. N. *Dynamic mechanical and thermal properties of MAPE treated jute/HDPE composites*. Compos Sci Technol, 2006, 66: 538-547.

[8] Corrales F., Vilaseca F., Llop M., Giromes J., Mendez J. A., Mutje P. *Chemical modification of jute fibers for the production of green-composites*. J Hazardous Mater, 2007, 44: 730-735.

[9] Ray D., Sarkar B. K., Rana A. K., Bose N. *The mechanical properties of vinylester resin matrix composites reinforced with alkali-treated jute fibers*. Composites: Part A, 2001, 32: 119-127.

[10] Stark N. *Influence of moisture absorption on mechanical properties of wood flour–polypropylene composites*. J Thermoplast Compos Mater,14:421–32, 2001.

[11] Marcovich N. E., Reboredo M. M., Aranguren M. I. *Dependence of the mechanical properties of woodflour–polymer composites on the moisture content*. J Appl Sci, 1998, 68:2069–76.

[12] Rangaraj S. V., Smith L. *Effects of moisture on the durability of a wood/thermoplastic composite*. J Thermoplast Compos Mater, 2000, 13(March):140–61.

[13] Lu J. Z., Wu Q., McNann H. S. *Chemical coupling in wood fiber and polymer composites: a review of coupling substances and treatment.* Wood Fiber Sci, 2000, 32(1):88–104.

[14] Nabi Saheb D., Jog J. P. *Natural fiber polymer composites: a review.* Adv Polym Technol, 1999, 18(4):351–63.

[15] Rozman H. D., Lee M. H., Kumar R. N., Abusanag A., Mohd. Ishak Z. A. *The effect of chemical modification of rice husk with glycidyl methacrylate on the mechanical and physical properties of rice husk–polystyrene composites*. J Wood Chem Technol, 2000, 93–109., 20(1):.

[16] Berthé V., Ferry L., Bénéze t J. C., Bergeret A. *Ageing of different biodegradable polyesters blends mechanical and hygrothermal behavior*. Polum Degrad Stabil, 2010, 95: 262-9.

[17] Shubhra Q. T. H., Alam A. K. M. M., Beg M. D. H. *Mechanical and degradation characteristics of natural silk fiber reinforced gelatin composites.* Mater Lett, 2011, 65:333–6.

[18] Dhakal H., Zhang Z., Richardson M. *Effect of water absorption on the mechanical properties of hemp fibre reinforced unsaturated polyester composites.* Compos Sci Technol, 2007, 67:1674–83.

[19] Methacanon P., Weerawatsophon U., Sumransin N., Prahsarn C., Bergado D. T. *Properties and potential application of the selected natural fibers as limited life geotextiles*. Carbohydr Polym, 2010, 82:1090–6.

[20] Joseph P. V., Rabello M. S., Mattoso L. H. C., Joseph K., Thomas S. *Environmental effects on the degradation behaviour of sisal fibre reinforced polypropylene composites.* Compos Sci Technol, 2002, 62:1357–72.

[21] Beg M. D. H., Pickering K. L. *Accelerated weathering of unbleached and bleached kraft wood fibre reinforced polypropylene composites*. Polym Degrad Stabil, 2008, 93:1939–46.

[22] Assarar M., Scida D., El Mahi A., Poilâne C., Ayad R. *Influence of water ageing on mechanical properties and damage events of two reinforced composite materials: flax–fibres and glass–fibres*. Mater Des, 2011, 32:788–95.

[23] Chen H., Miao M., Ding X. *Influence of moisture absorption on the interfacial strength of bamboo/vinyl ester composites*. Compos A Appl Sci Manuf, 2009, 40:2013–9.

[24] Z. N. Azwa, B. F. Yousif, A. C. Manalo, W. Karunasena. *A review on the degradability of polymeric composites based on natural fibres*. Materials and Design 47, 2013, 424–442.

[25] Mulder M., "Principles of Membrane technology". Kluwer Academic Publishers, Dordrech, Holland, 1991.

[26] Comyn J., "Polymer permeability". Elsevier Applied Science, New York, 1985.

[27] Paul D. R., Yampolskii Y. P., "Polymeric Gas Separation Membranes". CRC Press, Boca Raton, 1991.

[28] Schliecker G., Schmidt C., Fuchs St., Kissel T. *Characterization of a homologous series of D,L-lactic acid oligomers; a mechanistic study on the degradation kinetics in vitro*. Biomaterials, 2003, 24(21):3835-44

[29] Siepmann J., Göpferich A. *Mathematical modelling of bioerodible, polymeric drug delivery systems*. Adv Drug Delivery Rev, 2001, 48(2-3):229-47.

[30] de Jong S.J., Arias E.R., Rijkers D.T.S., van Nostrum C.F., Kettenes-van den Bosch J.J., Hennink W.E.. *New insights into hydrolytic degradation of poly(lactic acid): participation of the alcohol terminus*. Polymer, 2001, 42(7):2795-802.

[31] Fischer E.W., Sterzel H.J., Wegner G. *Investigation of structure of solution grown crystals of lactide copolymers by means of chemical-reactions*. Kolloid Z. Z. Polym, 1973, 251(11):980-90.

[32] Heya T., Okada H., Ogawa Y., Toguchi H. *In-vitro and in-vivo evaluation of thyrotropin-releasing-hormone release from copoly(DL-lactic/glycolic acid) microspheres*. J Pharm Sci, 1994, 83(5):636-40.

[33] Shih C. *A graphical method for the determination of the mode of hydrolysis of biodegradable polymers*. Pharm Res, 1995, 12(12):2036-40.

[34] Aso Y., Yoshioka S., Li Wan Po A., Terao T. *Effect of temperature on mechanisms of drug-release and matrix degradation of poly(D,L-lactide) microspheres*. J Controlled Release, 1994, 31(1):33-9.

[35] David K., Yang Y.Q. *Molecular modeling study of the resistance of PLA to hydrolysis based on the blending of PLLA and PDLA*. Polymer, 2006, 47:4845–50.

[36] Thwe M.M., Liao K. *Durability of bamboo-glass fiber reinforced polymer matrix hybrid composites. Compos Sci Technol*, 2003, 63:375–87.

[37] Lu X., Zhang M.Q., Rong M.Z., Yue D.L., Yang G.C. *Environmental degradability of self-reinforced composites made from sisal*. Compos Sci Technol, 2004, 64:1301–10.

[38] George J., Bhagawan S.S., Thomas S. *Effects of environment on the properties of low-density polyethylene composites reinforced with pineapple-leaf fibre*. Compos Sci Technol, 1998, 58:1471–85.

[39] Espert A., Vilaplana F., Karlsson S. *Comparison of water absorption in natural cellulosic fibres from wood and one-year crops in polypropylene composites and its influence on their mechanical properties*. Compos Part A, 2004, 35:1267–76.

[40] Arbelaiz A., Fernández B., Ramos J.A., Retegi A., Llano-Ponte R., Mondragon I. *Mechanical properties of short flax fibre bundle/polypropylene composites: Influence of matrix/fibre modification, fibre content, water uptake and recycling*. Compos Sci Technol, 2005, 65:1582–92.

[41] Bledzki A.K., Gassan J. *Composites reinforced with cellulose based fibers*. Prog Polym Sci, 1999, 24:221–74.

[42] Asociación Española de Normalización y Certificación (AENOR). http://www.aenor.es. (2011)

[43] Yew G. H., Mohd Yusof A. M., Mohd Ishak Z. A., Ishiaku U. S. *Water absorption and enzymatic degradation of poly(lactic acid)/rice starch composites*. Polym Degrad Stabil 90, 2005, 488-500.

[44] Wang H., Sun X. Z., Seib P. *Strengthening blends of poly(lactic acid) and starch with methylenediphenyl diisocyanate*. J Appl Polym Sci, 2001, 82:1761-7.

[45] Bismarck A., Askargorta I. A., Springer J., Lampke T., Wielage B., Stamboulis A. *Surface characterization of flax, hemp and cellulose fibres, 2002, surface properties and the water uptake behaviour*. Polym Compos, 23:872–94.

[46] J. D. Badia, L. Santonja-Blasco, A. Martínez-Felipe, A. Ribes-Greus. *Hygrothermal ageing of reprocessed polylactide*. Polym Degrad Stabil, 2012, 97:1881-1890.

[47] Neogi P.. "Diffusion in polymers", Marcel Dekker, New York, 1996, 71.

[48] Tang C. Y., Chen D. Z., Yue T. M., Chan K. C., Tsui C. P., Peter H. F. Yu. *Water absorption and solubility of PHBHV/HA nanocomposites*. Compos Sci Technol, 2008, 68:1927-1934.

[49] Braden M., Causton E. E. , Clarke R. L. *Diffusion of water in composite filling materials*. J Dent Res, 1976, 55:730–2.

[50] Fischer E. W., Sterzel H. J., Wegner G. *Investigation of structure of solution grown crystals of lactide copolymers by means of chemical-reactions*. Kolloid Z Z Polym, 1973, 251(11):980-90.

[51] Aso Y., Yoshioka S., Li Wan Po A., Terao T. *Effect of temperature on mechanisms of drug-release and matrix degradation of poly(D,L-lactide) microspheres*. J Controlled Release, 1994, 31(1):33-9.

[52] Suryanegara, L., Nakagaito, A. N., & Yano, H. (2009). *The effect of crystallization of PLA on the thermal and mechanical properties of microfibrillated cellulose-reinforced PLA composites.* Compos Sci Technol, 69, 1187–1192.

[53] Papageorgiou G. Z., Achilias D. S., Nanaki S., Beslikas T., Bikiaris D.. *PLA nanocomposites: Effect of filler type on non-isothermal crystallization*. Thermochimica Acta 511, 2010, 129-139.

[54] Fairbridge C., Ross R. A., Sood S. P.. *A kinetic and surface study of the thermal decomposition of cellulose powder in inert and oxidizing atmospheres*. J App Polym Sci , 1978. 22(2):497-510.

[55] Adriana R. Martina, Maria Alice Martinsb, Odilon R.R.F. da Silva, Luiz H. C. Mattosod, *Studies on the thermal properties of sisal fiber and its constituents*. Thermochimica Acta, 2010, 506:14–19.

[56] C. Albano, J. González, M. Ichazo, D. Kaiser. *Thermal stability of blends of polyolefins and sisal fiber*. Polym Degrad Stabil, 1999, 66:179-190.

Acknowledgements

First of all, I would thank to my supervisors. I am grateful to Dr. Amparo Ribes Greus (Universitat Politècnica de València) for her guidance, help and support during the development of this project. Thank you for giving me the opportunity and believe in me as a member of your group. I am also thankful to Dr. Xavi Ramis Juan (Universitat Politècnica de Catalunya) for his assistance and making possible collaboration between both Universities.

I would like to specially thank to the one who has guided me along my short career as investigator, Dr. Jose David Badia Valiente. Thank you for your entire dedication and attention.

In addition, I give my sincere gratitude to all the people who have encouraged and supported me during this period; particularly, to all the members of the group: Alf, Soraia, Marta, Roberto and Carlos.

Thank you, family for being there always I have needed it. You have taught me how to deal and overcome daily and occasional difficulties and I really appreciate it.